Earth System Model Evaluation Tool (ESMValTool) v2.0 – diagnostics for emergent constraints and future projections from Earth system models in CMIP

Axel Lauer[1], Veronika Eyring[1,2], Omar Bellprat[3], Lisa Bock[1], Bettina K. Gier[2,1], Alasdair Hunter[5], Ruth Lorenz[4], Núria Pérez-Zanón[5], Mattia Righi[1], Manuel Schlund[1], Daniel Senftleben[1], Katja Weigel[2,1], and Sabrina Zechlau[1]

[1]Deutsches Zentrum für Luft- und Raumfahrt (DLR), Institut für Physik der Atmosphäre, Oberpfaffenhofen, Germany
[2]University of Bremen, Institute of Environmental Physics (IUP), Bremen, Germany
[3]Swiss Federal Department of Foreign Affairs, Bern, Switzerland
[4]ETH Zurich, Institute for Atmospheric and Climate Science, Zurich, Switzerland
[5]Barcelona Supercomputing Center (BSC), Barcelona, Spain

Correspondence to: A. Lauer (Axel.Lauer@dlr.de)

In the following we address the comments of reviewer #1 and reviewer #2 during the open discussion of the paper ”Earth System Model Evaluation Tool (ESMValTool) v2.0 – diagnostics for emergent constraints and future projections from Earth system models in CMIP”. We would like to thank the two anonymous reviewers for the time and effort reviewing the paper. We feel it has improved thanks to the constructive comments. We have listed all reviewers’ comments below and our answers are provided in blue. All line numbers refer to the ”track changes” version of the revised manuscript attached to this document.

The following point-by-point response is identical to the replies to the reviewers’ comments posted on the ”interactive discussion” and includes all relevant changes made in the manuscript.

Anonymous Referee #1

The authors present a description of the latest version of ESMValTool, including details on the new evaluation metrics and 'recipes' that are included. These are clearly linked to the original publications which describe the metrics and examples are provided. This is a clear and well structured paper that I am happy to recommend be published with only minor changes.

We thank Reviewer #1 for providing helpful comments to improve the manuscript.

I do have two minor comments on the tool and its presentation here. The first is regarding the recipe names which seem somewhat arbitrary. It might be clearer if they followed a standardised format. The other comment is on the various example emergent constraint plots. While it's certainly useful to be able to directly compare with the published work, the very different plot styles jars slightly when presented together like this. Would it be possible to make the original paper formatting of the plots optional, otherwise reverting to a single consistent format? Would it also be possible to add R^2 values to the plots to indicate how well a linear fit really captures the relationship in the models?

The used naming convention for all recipes that are based on a single peer-reviewed publication or report is recipe_FirstAuthorName_Yea e.g. recipe_deangelis15nat.yml. However, for recipes that are based on multiple papers, we relaxed this convention leaving it up to the authors of the diagnostics to decide on a meaningful name, e.g. recipe_seaice.yml combines different diagnostics for sea ice that are based on various articles. An example not fully fitting into either of these categories is recipe_toymodel.yml. In these cases, the naming convention has also been relaxed to any descriptive term chosen by the authors of the diagnostic. The emergent constraints shown in Figures 6, 7, 8, 9, and 10 have been programmed by different authors (in different languages) as contributions to different projects. In order to give the scientists contributing to the ESMValTool as much freedom as possible and to keep the bar for contributions as low as possible (which is admittedly already quite high) we consider this fine. Homogenizing these figures would require significant recoding. All these diagnostics do, however, output the results as netCDF files, so any plotting program could be used with the ESMValTool output to produce additional plots in the format and layout as desired. Following the suggestion of the reviewer, we added the R^2 values to all panels of Figure 6.

Other, minor, grammatical comments: L5: "...implemented include ECS..." -> "...implemented include constraints on ECS..." L195: "used as emergent constraint." -> "used as an emergent constraint."

Changed as suggested.

Anonymous Referee #2

This paper describes part of the functionality of the ESMval tool that can be used to evaluate and intercompare CMIP (and other) model data. Tools that automate part of the process of collocating and analysing data are immensely useful as they increase efficiency, avoid redundancy and minimise the risk of errors. Given the ever larger flow of (model) data these tools can rightfully be considered part of our modelling toolkit. GMD is an appropriate choice of journal for this paper. The paper has a clear structure and is well written although sometimes short on detail.

We also thank Reviewer #2 for helping us to improve the manuscript.

The paper states that its aim is "to document and illustrate [] these newly added ESMValTool ”recipes”. However, very little information is given to the user on how to use these ’recipes’ (do we need to set certain parameters? how does the code find the data? What requirements are there for the data, both models and observations?). Rather the paper seems more an advertisement than a technical document (see https://www.geosci-model-dev.net/9/3093/2016/gmd-9-3093-2016.pdf for an example of the latter). This is not necessarily bad but the paper does not make it easy for users to find the technical documents to obtain this information. As a side note: the readme for the tutorial on github is mostly unpopulated.

In contrast to the tool documentation example given by the reviewer, the documentation of the new features of the ESMValTool would be (in our opinion) too extensive for a single paper. We therefore decided to split the technical description of the tool and its preprocessor and the scientific description of the new diagnostics and metrics grouped by main application. All of the reviewer’s questions regarding data format, directory structure, file names, settings of certain parameters, etc. are covered by our companion paper Righi et al., GMD, 13, 1179-1199, 2020, to which we refer for technical details in this paper. We agree with the reviewer that it should be as easy as possible for the reader to find the technical documents. We therefore we added the following paragraph to the beginning of section 3 (lines 118-124):

> ”All diagnostics output one or more netCDF file(s) containing the results of the analysis that are then visualized in the figure(s) created. The file format of the figures can be defined in the user configuration file and includes common formats such as png, pdf, ps and eps. For more details on the technical infrastructure of the tool including accepted data formats, data reference syntax (DRS) used for directory and file name conventions, available preprocessor functions, etc. we refer again to (Righi et al., 2020). Further information can be found in the ESMValTool user’s guide, which documents all technical aspects of the tool as well as all available diagnostics, see https://docs.esmvaltool.org/.”

The reviewer is correct the README on GitHub is quite brief. This is intentional as we think a very brief description of the main purpose of the tool and a link to the user’s guide is probably fine. The idea is that referring to the user’s guide instead of duplicating information from the user’s guide helps to avoid redundancies and reduces the risk of outdated documentation as everything is in one place.

Furthermore, I miss discussions of following topics:

- a discussion of the spatio-temporal resolution of the model data and observations used by ESMvaltool. P 3, l 83 states that ”any arbitrary model output” can be used. Is that really true? Can I use e.g. both yearly averaged data and hourly data?

  The tool itself (i.e. the preprocessor) can indeed handle all time and spatial resolutions that are defined in the CMOR tables for a specific CMIP phase. For CMIP6, for examples, this includes time resolutions from (sub-)hourly to yearly and regular as well as irregular latitude-longitude grids. The diagnostics, however, often expect a certain time resolution or require data to be on a regular latitude-longitude grid or on given pressure levels. This is defined by the diagnostic authors and typically depends on the main aim of the diagnostic.

- a discussion of the tool’s expectation when it comes to the format of observational data. Presumably these should be gridded.

  The tool expects all input data including observations to follow the CMOR standard (as outlined in section 2). Typically, such data are stored on a regular (i.e. Cartesian longitude-latitude) grid. The CMOR standard also allows for non-Cartesian longitude-latitude grids if the grid and its mapping parameters are defined. For clarification, we added web links for CF, CMOR and the CMOR tables and definitions used in CMIP6 to section 2.

- a description of how ESMvaltool deals with differences in the spatio-temporal resolutions between datasets. This is alluded to in a single Figure caption but should be clearly stated in the paper as part of the tool’s functionality. As a side note, it appears the authors believe that observational errors are all stand in the way of model evaluation but there are two other issues. These are 1) differences in spatiotemporal sampling of different datasets and the representativity issues that result (see e.g. https://www.atmos-chem-phys.net/17/9761/2017/ and the references therein); 2) appropriateness of the observation operator (i.e. the model’s code that generates a diagnostic that may be compared to observations, e.g. what definition of temperature is used?).

  Regarding regridding, we added the following paragraph to section 3.1 (lines 129-135):

  > ”For this, all data are regridded to the same horizontal grid. In the example shown in Figure 1, all models are regridded to the grid of BCC-CSM1-1 using a linear interpolation scheme. This task is done by the ESMValTool’s preprocessor and defined in the recipe depending on the application and user requirements. The user-definable configuration options include definition of the target grid (e.g. 2.5°x2.5°) and regridding scheme (e.g. linear, nearest, area weighted). Regridding/interpolation of the input data in time is currently not supported. For further details we refer to the ESMValTool user’s guide (https://docs.esmvaltool.org/).”

  Regarding observational errors, the reviewer has a good point. We therefore extended section 3.4.2 briefly mentioning additional sources of uncertainty when comparing observations to models (lines 450-458):

> ”We would like to note that in addition to the observational uncertainty itself, also spatio-temporal representativeness of observations plays an important role when evaluating models. Schutgens et al. (2017) showed that such representation errors remain even after spatial and temporal averaging and may be larger than typical measurement errors. In addition, also the calculation method of a quantity to be compared with observations can play an important role. This is, for example, the case when comparing satellite retrievals with model quantities that are not derived the same way. Application of satellite simulators such as the Cloud Feedback Model Intercomparison Project (CFMIP) Observation Simulator Package (COSP; Bodas-Salcedo et al. (2011)) can help to reduce such uncertainties in model evaluation. Both of these aspects are not covered by the toy model, that only provides an estimate for the observational uncertainty itself.”

- a discussion of the underlying assumptions in the many regressions used by the tool. My guess is that one important assumption is that individual models can be viewed as independent data points which is unlikely given that often models share (part of) their code base or at the very least incoporate similar ideas with regards to e.g. sub-grid parametrisations.

  The reviewer is correct that an underlying assumption of the regressions (used for the emergent constraints) is that the individual models are independent. The reviewer is also correct that as some modeling groups provide output from multiple ESMs and even some ESMs from different modeling groups share components or code, the models are clearly not independent. Duplicated code as well as identical forcing and validation data in multiple models is expected to lead to an overestimation of the sample size of a model ensemble and may result in spurious correlations.

  The original studies proposing the emergent constraints shown here do not explicitly take into account model interdependency. As the aim of this implementation was to be able to reproduce the original studies, we did not change this assumption. As the reviewer has a good point, we added the following paragraph to section 3.3:

  > ”We would like to note that a limitation of the emergent constraints as currently implemented into the ESMValTool is that model interdependency, as in the original studies, is not explicitly taken into account. As some modeling groups share model components or code the models are not all independent. Duplicated code as well as identical forcing and validation data in multiple models is expected to lead to an overestimation of the sample size of a model ensemble and may result in spurious correlations (Sanderson et al., 2015). As a possible approach future implementations of these emergent constraints could, for example, apply a model weighting based on a model’s interdependence (e.g. Knutti et al., 2017) or simply reduce the ensemble size taking into account models only that are above a given yet to be defined interdependence score.”

- a mention of the graphics formats produced by the tool and whether the user has any control over them.

  We added the supported graphics formats to the beginning of section 3 (see our answer to the reviewer’s first comment).

Finally, I think there may be substantial mistakes in Sect. 3.4.2 that need to be addressed. In addition I found it lacked sufficient explanation.

Minor comments:

Should Table 1 maybe have more information on e.g. the temporal averaging in model data that is needed or do the scripts work with high-freuqency output and perform this averaging themselves?

We corrected the mistakes in Sect. 3.4.2 and added some clarifications and explanations (see our answers to the detailed comments below). Thanks for spotting the mistakes.

All of the diagnostics listed in table 1 expect time series of monthly mean data as input. We added this information to the caption of table 1.

p. 3, l. 80-85: Can the authors provide references (even if weblinks) for CF-complaincy and CMOR?

We added web links for CF, CMOR and the CMOR tables and definitions used in CMIP6.

p. 3, l. 90: Apparently users can 'import' their own favouite datasets and use them with ESMValtool. Can the authors provide a brief description of the steps necessary for this to work?

As suggested, we added more details on including non-CMOR-like observational datasets into the ESMValTool to section 2 (lines 99-109):

> "Such other datasets that are not available via the obs4mips (https://esgf-node.llnl.gov/projects/obs4mips/) or ana4mips (https://esgf.nccs.nasa.gov/projects/ana4mips/) projects and for which no cmorizing scripts are provided can be used with the ESMValTool in two ways. The first is to write a new cmorizing script using an available one as a template to generate a local copy of reformatted data that can readily be used with the ESMValTool. This typically involves saving only one variable per file and adding meta data such as coordinates (e.g. longitude, latitude, pressure level, time) and attributes (e.g. variable standard and long names, units, dimensions) according to the CMOR standard to the dataset(s). The second way is to implement specific 'fixes' for this dataset in which case the cmorizing is performed 'on the fly' during the execution of an ESMValTool recipe. For details on both methods we refer to the ESMValTool user's guide available at https://docs.esmvaltool.org/en/latest/input.html#observations."

p 5, l 139,140: I do not know whether tas and rlut etc belong to CF-compliant or CMOR definitions but can the authors clarify, also where readers may find further definitions?

These so-called "standard names" of variables (e.g. tas, rlut, etc) are defined in the CMOR tables read in by the ESMValTool. In addition to web links to the CF and CMOR standards, we also added the following sentence on the CMOR tables to section 2 (lines 91-93):

> ”These tables read in by the ESMValTool contain the definition of all variables, together with their metadata such as units and standard and long names.”

p 7, l 189: ’correlation of the covariance’. Shouldn’t this just be ’correlation’?

Thanks for spotting this. Corrected as suggested.

p 13, Sec. 3.4.2: I suggest there is something wrong with either the equation or the definitions here. When alpha=1, the eps$_{i,m}$ would be drawn from a distribution with imaginary (!) standard deviation (unless beta=0).

We thank the reviewer for noticing this lack of information that has been addressed by adding (line 435):

> ”[. . .] β being limited to the range $0 \leq \beta \leq \sqrt{1-\alpha^2}$.”

There are numerous other issues with this section:

- x$_i$ is (probably) not an observation but an anomaly (y has mean 0).

  We thank the reviewer for noticing this point. Since the goal of this diagnostic is to simulate single-model ensembles from an observational dataset to investigate the effect of observational uncertainty, the word ”observations” is used to distinguish from the model output. It is also used following Weigel et al. (2008) who describe the method.

  Given that the recipe does not compute the anomaly itself as an extension of the method described in Weigel et al. (2008), we have modified the parameters of y to cover all possibilities to ”y $\sim$ N(μ,1)”. In the ESMValTool implementation, the user can choose between two options: using the original variable or its anomaly.

- How is the ’mean correlation between a series of values (x$_{i,1..M}$) and a single value (y$_i$) defined?

  It is a property of the toy model described in Weigel et al. (2008): ”The average correlation coefficient between the forecast ensemble members and the observations is prescribed by a model parameter α.”. As a clarification, we added ”(see toy model properties described in Weigel et al., 2008)” to bullet point #2 (lines 431-432).

- What is the meaning of eps$_{i,m}$? Note: it is also called eps$_i$ sometimes (l. 383), please correct this.

  Thanks again for reporting this problem. The text has been corrected adding that ϵ_m is a vector of perturbations and ϵ_β scalar perturbation (line 428):

  > ”The simulated value xm is obtained by multiplying y by α, the predictability of the observation, which is set to 1 in this instance, and by adding a vector of perturbations ϵ_m and the scalar perturbation ϵ_β.”

- I’m not familar with the work by Weigel but it seems odd to call alpha the predictability. Don’t the random errors eps control the predictability? Probably I misunderstand something but it appears that, beyond the correction of aforementioned errors, this section needs much more explanation.

We agree with the reviewer that much more explanation could improve this section and we want also to keep the description simple to make users understand the aim of the metric while deeper understanding could be obtained from the main reference Weigel et al. (2008). Therefore, we added the following sentence as a clarification on α and the predictability (lines 436-439):

> ”Parameter β is introduced to control the dispersion. For well-dispersed ensembles, skill is independent of the number of simulations involved, while for overconfident model ensembles, skill grows with the ensemble size. Given that β accounts for the dispersion, this approach leads α to represent a measure of predictability (Weigel et al., 2008).”

- the purpose of the toy model is not really explained. I guess it allows the user to put an error estimate on the uncertainty of observations used in emergent constraints etc? Can the user apply this toy model to every constraint or are there limitations? What underlying assumption feed into this toy model? Independent and Identically randomly distributed errors is probably a major assumption and needs to be written down explicitly!

  As suggested, we added the list of assumptions made (lines 440-444):

  > ”This toy model is based on very simplifying assumptions: (1) normality and stationarity, the climatology and the ensemble distributions are assumed to be stationary and normally distributed; (2) well-calibrated model climatology, each ensemble member has the same climatology as the observations; (3) stationary skill, spread and correlation do not vary from sample to sample; (4) predictable signal and observational errors, requires the signal to be given by αx, and therefore it is determined by the verifying observation (Weigel et al., 2008).”

- Toy model may be a confusing choice of word, as the ESMval tool is all about model evaluation. Maybe uncertainty simulator (or estimator) would be a better choice?

  We would prefer to keep the name of the recipe for two reasons: (1) ”toymodel” is the name used in Weigel et al. (2008); (2) the name is already in use by the software of the MAGIC portal (Copernicus Climate Change Service).

p 14, l 409: ”including stippling and hatching to indicate significant changes and areas where models do not agree” I found this sentence onfusing. It suggests that stippling/hatching is used to indicate where models do not agree but the caption to Fig 18 states otherwise. Elsewhere in the paper stippling/hatching is used to indicate agreement as well.

In order to clarify the use of stippling and hatching, we reformulated this phrase as follows (lines 471-473):

> ”including stippling to indicate large changes with high model agreement and hatching to indicate areas with a small signal or low agreement of models”

p 14, l 412: ”where the projections are still uncertain (hatching).” It appears that the use of hatching is quite inconsistent. I understand that the authors are trying to recreate figures found in a large number of papers that are unlikely to be consistent.

Maybe this is something to note in the summary or elsewhere, e.g. a 'buyer be ware' clause. After all the authors provide a single tool to generate figures that will be assumed by most users to be consistent in their definitions.

Hatching is used throughout the paper to indicate a small signal or low agreement of models. In order to clarify this, we extended this sentence (lines 476-478):

> "This example also shows quite large regions where the projections are still uncertain, i.e. the multi-model mean signal is smaller than one standard deviation of the natural variability estimated from preindustrial control simulations (hatching)."

p 15, l 444-446: this explanation of other papers regarding ESMval should be part of the introduction, in my opinion. I would also suggest to add more detail: as a user I want to know which paper to use to find what information.

As suggested, we moved this paragraph to the introduction (lines 52-59).

p 15, Sect 4: I suggest removing the names of recipes. The serve no purpose in this summary.

Changed as suggested.

p 15, Sect 4: The summary should contain a brief mention of data requirements and limitations of the tool. As it stands it is a brief rehashing of the the list of emergent constraints and nothing more.

Following the reviewer's suggestions, we extended the summary section adding the following paragraph on the ESMValTool's data requirements and limitations (lines 568-582):

> "The ESMValTool v2.0 is an open source software tool that has been specifically developed to facilitate evaluation and analysis of Earth system models participating in CMIP. As such, it can process and analyze CMOR compliant model output and observational datasets with the particular aim to provide traceable and reproducible results, well-documented diagnostics and metrics and an efficient workflow allowing to evaluate models in more depth and more rapidly than it was typically possible in previous CMIP phases. The CMOR standard is, however, quite detailed and implemented in a relatively strict way in the ESMValTool in order to ensure data consistency and to minimize the probability of errors in the data processing. Increasing the flexibility of the CMOR check and automatic fixes of small inconsistencies is a currently ongoing activity and should make the data processing smoother, especially for datasets which are not part of CMIP or any CMIP-Endorsed-Model-Intercomparison-Project (MIP). This means that a certain familiarity with these data standards is required in order to use the ESMValTool. Another limitation is that for license issues, observations cannot be distributed together with the software package. New users are required to download and process observational datasets before being able to use the tool or to have access to

a computing center where observational data for the ESMValTool (i.e. cmorized) are already available. We are currently working on automating this process to facilitate the data retrieval and cmorization process.”

Earth System Model Evaluation Tool (ESMValTool) v2.0 – diagnostics for emergent constraints and future projections from Earth system models in CMIP

Axel Lauer[1], Veronika Eyring[1,2], Omar Bellprat[3], Lisa Bock[1], Bettina K. Gier[2,1], Alasdair Hunter[5], Ruth Lorenz[4], Núria Pérez-Zanón[5], Mattia Righi[1], Manuel Schlund[1], Daniel Senftleben[1], Katja Weigel[2,1], and Sabrina Zechlau[1]

[1]Deutsches Zentrum für Luft- und Raumfahrt (DLR), Institut für Physik der Atmosphäre, Oberpfaffenhofen, Germany
[2]University of Bremen, Institute of Environmental Physics (IUP), Bremen, Germany
[3]Swiss Federal Department of Foreign Affairs, Bern, Switzerland
[4]ETH Zurich, Institute for Atmospheric and Climate Science, Zurich, Switzerland
[5]Barcelona Supercomputing Center (BSC), Barcelona, Spain

Correspondence to: Axel Lauer (axel.lauer@dlr.de)

Abstract

The Earth System Model Evaluation Tool (ESMValTool), a community diagnostics and performance metrics tool for evaluation and analysis of Earth system models (ESMs) is designed to facilitate a more comprehensive and rapid comparison of single or multiple models participating in the ~~c~~Coupled ~~m~~Model ~~i~~Intercomparison ~~p~~Project (CMIP). The ESM results can be compared against observations or reanalysis data as well as against other models including predecessor versions of the same model. The updated and extended version 2.0 of the ESMValTool includes several new analysis scripts such as large-scale diagnostics for evaluation of ESMs as well as diagnostics for extreme events, regional model and impact evaluation. In this paper, the newly implemented climate metrics such as effective climate sensitivity (ECS) and transient climate response (TCR) as well as emergent constraints for various climate-relevant feedbacks and diagnostics for future projections from ESMs are described and illustrated with examples using results from the well-established model ensemble CMIP5. The emergent constraints implemented include constraints on ECS, snow-albedo effect, climate-carbon cycle feedback, hydrologic cycle intensification, future Indian summer monsoon precipitation, and year of disappearance of summer Arctic sea ice. The diagnostics included in ESMValTool v2.0 to analyze future climate projections from ESMs further include analysis scripts to reproduce selected figures of chapter 12 of the Intergovernmental Panel on Climate Change's (IPCC) Fifth Assessment report (AR5) and various multi-model statistics.

1 Introduction

Climate models are important tools not only to improve our understanding of the key processes in present-day climate but also to project future climate change under different plausible scenarios. Climate models have been continuously improved and extended over the last decades from relatively simple atmosphere-only models to the complex state-of-the-art Earth system models (ESMs) participating in the latest (sixth) phase of the Coupled Model Intercomparison Project (CMIP6, Eyring et al. (2016a)). The increasing complexity of the models is needed to represent key feedbacks that affect climate change, but is also likely to increase the spread of climate projections across the multi-model ensemble (Eyring et al., 2019). This poses a challenge for evaluation and analysis of the model results that requires efficient tools able to handle the increasing number of variables, processes and also the increasing data volume.

The ESMValTool released in a first version in 2016 (Eyring et al., 2016b) has been developed with the aim of taking model evaluation to the next level by facilitating analysis of many different ESM components, providing well-documented source code and scientific background of implemented diagnostics and metrics and allowing for traceability and reproducibility of results (provenance). This has been made possible by a lively and growing development community continuously improving the tool supported by multiple national and European projects. The release of version 2.0 (v2.0) of the ESMValTool ~~that is documented in this and accompanying papers (Eyring et al., in review; Righi et al., 2020; Weigel et al., in prep.)~~ has been developed as a large community effort to specifically target the increased data volume of CMIP6 and the related challenges posed by analysis and evaluation of output from multiple high-resolution and complex ESMs.

For this, the core functionalities have been completely rewritten in order to take advantage of state-of-the-art computational libraries and methods to allow for faster, more efficient and user-friendly data processing (Righi et al., 2020). Besides many technical improvements ESMValTool v2.0 includes new large-scale diagnostics for evaluation of Earth system models (Eyring et al., in review) and diagnostics for extreme events, regional model and impact evaluation and analysis of ESM results (Weigel et al., in prep.). As part of a series of four articles describing the new features and diagnostics of the Earth System Model Evaluation Tool v2.0, this paper ~~The new version of the ESMValTool now also~~ focuses on the newly included~~s~~ diagnostics for emergent constraints and for analysis of future projections from ESMs~~ that are described in this article~~ as well as~~. Additionally, v2.0 includes~~ multi-model products (Sect. 3.1) and the two new climate metrics effective climate sensitivity (ECS) and transient climate response (TCR) (Sect. 3.2).

An emergent constraint is a relationship across an ensemble of models between some aspect of the Earth system sensitivity and an observable trend or variation in the current climate, which offers the possibility to reduce uncertainties in climate projections. Furthermore, emergent constraints can help guiding model development onto processes crucial to the magnitude and spread of future climate change projections and to point out future observational priorities (Eyring et al., 2019). Emergent constraints implemented in ESMValTool v2.0 (Sect. 3.3) include seven different approaches to constrain ECS as well as constraints for the hydrological cycle intensification, snow-albedo effect, year of disappearance of summer Arctic sea ice, future Indian summer monsoon precipitation and climate-carbon cycle feedback.

For the analysis of ESM projections, ESMValTool v2.0 now includes diagnostics to reproduce selected figures from chapter 12 (Long-term Climate Change: Projections, Commitments and Irreversibility) of the ~~Intergovernmental Panel on Climate Change's (~~IPCC~~) Fifth Assessment report (~~ AR5~~)~~ (Collins et al., 2013). These include figures showing the change in a variable between historical and future periods, e.g. maps (2D variables), zonal means (3D variables), time series showing the change in certain variables from historical to future periods for multiple scenarios, and maps visualizing change in variables normalized by global mean temperature change (pattern scaling) and the possibility to show statistical significance of changes when compared to natural variability and the degree of agreement between the models using the stippling and hatching methods as in Collins et al. (2013). Furthermore, diagnostics tailored to analyze projections of sea ice such as, for example, calculation of the year of disappearance (sea ice extent below 1 million km^2) from a multi-model ensemble and to constrain the future austral jet position have been added. A newly implemented "toy model" can be used to generate synthetic members of a single dataset. When providing an estimate for the standard error of observations e.g. from differences between different observational datasets, this toy model can be used to investigate and take into account the effect of observational uncertainty in model evaluation (Sect. 3.4). A summary is given in Sect. 4. The aim of this paper is to document and illustrate how these newly added ESMValTool “recipes”, i.e. configuration files defining input, preprocessing, diagnostics and run-time options of the ESMValTool, can be used for model evaluation and analysis.

2 Models and observations

The open-source release of ESMValTool (v2.0) that accompanies this paper is intended to work with CMIP5 and CMIP6 model output (and partly also with CMIP3 if the required output has been generated~~saved~~), but the tool is compatible with any arbitrary model output, provided that it is in CF-compliant (CF = Climate and Forecast, http://cfconventions.org/) netCDF format and that the variables and metadata are following the CMOR (Climate Model Output Rewriter, https://pcmdi.github.io/cmor-site/media/pdf/cmor_users_guide.pdf) tables and definitions (e.g. https://github.com/PCMDI/cmip6-cmor-tables/tree/master/Tables for CMIP6). These tables read in by the ESMValTool contain the definition of all variables, together with their metadata such as units and standard and long names. Observations used in the evaluation are detailed in the various sections of the manuscript (see also Section 6) and summarized in Table 1~~Table 1~~ and Table 2~~Table 2~~ but should also be seen as examples as they can be easily replaced by other observational datasets provided they follow the CMOR convention. For selected observational datasets, cmorizing~~reformat~~ scripts are provided with the ESMValTool that contain detailed downloading and processing instructions to convert the datasets into a CMOR-like format that can be processed by the ESMValTool. These reformat scripts serve as examples for writing similar scripts for other observational datasets that do not follow the CMOR standard. Such other datasets that are not available via the obs4mips (https://esgf-node.llnl.gov/projects/obs4mips/) or ana4mips (https://esgf.nccs.nasa.gov/projects/ana4mips/) projects and for which no cmorizing scripts are provided can be used with the ESMValTool in two ways. The first is to write a new cmorizing script using an available one as a template to generate a local copy of cmorized data that can readily be used with the ESMValTool. This typically involves saving only one variable per file and adding meta data such as coordinates (e.g. longitude, latitude, pressure level, time) and attributes (e.g. variable standard and long names, units, dimensions) according to the CMOR standard to the dataset(s). The second way is to implement specific ‘fixes’ for this dataset in which case the cmorizing is performed ‘on the fly’ during the execution of an ESMValTool recipe. For details on both methods we refer to the ESMValTool user’s guide available at https://docs.esmvaltool.org/en/latest/input.html#observations.

3 Overview of recipes included in ESMValTool v2.0 for emergent constraints and future projections

In this section, all diagnostics and metrics newly added to the ESMValTool v2.0 for analysis of future projections from ESMs as well as the emergent constraints implemented are described and illustrated with examples using results from the CMIP5 model ensemble (Taylor et al., 2012). The ESMValTool workflow is controlled by configuration files called “recipes”, which define all input datasets, pre-processing steps and diagnostics to run (for details we refer to Righi et al. (2020)). An overview of all recipes described in this paper including a short description, the variables processed, the names of the diagnostic scripts and observations is given in Table 1~~Table 1~~.

All diagnostics output one or more netCDF file(s) containing the results of the analysis that are then visualized in the figure(s) created. The file format of the figures can be defined in the user configuration file and includes common formats such as png, pdf, ps and eps. For more details on the technical infrastructure of the tool including accepted data formats, data reference syntax (DRS) used for directory and file name conventions, available preprocessor functions, etc. we refer again to (Righi et al., 2020). Further information can be found in the ESMValTool user's guide, which documents all technical aspects of the tool as well as all available diagnostics, see https://docs.esmvaltool.org/.

3.1 Calculations of multi-model products

Multi-model means are commonly used to project climate change (IPCC, 2013, 2007) and are thus a useful quantity to calculate in support of diagnostics included in the ESMValTool.

The recipe *recipe_multimodel_products.yml* computes the multi-model ensemble mean for a set of models selected by the user for individual variables and different temporal resolutions (annual, seasonal, monthly). For this, all data are regridded to the same horizontal grid. In the example shown in Figure 1, all models are regridded to the grid of BCC-CSM1-1 using a linear interpolation scheme. This task is done by the ESMValTool's preprocessor and defined in the recipe depending on the application and user requirements. The user-definable configuration options include definition of the target grid (e.g. 2.5°x2.5°) and regridding scheme (e.g. linear, nearest, area weighted). Regridding/interpolation of the input data in time is currently not supported. For further details we refer to the ESMValTool user's guide (https://docs.esmvaltool.org/). After selecting the region (rectangular region defined by the lowermost and uppermost longitudes and latitudes), the mean for the selected reference period is subtracted from the time series in order to obtain the anomalies for the desired period. In addition, the recipe computes the percentage of models agreeing on the sign of this anomaly, thus providing some information on the robustness of the climate change signal.

The output of the recipe consists of a contour map showing the time average of the multi-model mean anomalies and stippling to indicate locations where the percentage of models agreeing on the sign of the multi-model mean anomaly exceeds a threshold selected by the user (Figure 1~~Figure 1~~). The example in Figure 1~~Figure 1~~ shows a warming over the continents in the range of 1-2 K which is more pronounced than the warming over the ocean which is mostly in the range of 0.5-1.5 K in this scenario. The example also shows that the models largely agree on the sign of the temperature change with the most prominent exceptions found in parts of the Southern Ocean, Greenland and the North Atlantic. Furthermore, a time series of the area-weighted mean anomalies is plotted. For the plots, the user can select the length of the running window for temporal smoothing and choose to display either the ensemble mean with a light shading to represent the spread of the ensemble or ~~choose to display~~ each individual model separately (Figure 2~~Figure 2~~). The example in Figure 2~~Figure 2~~ shows an increase in global average June temperatures up to about 2060 when temperatures start to level off. By 2100 the four CMIP5 example models MPI-ESM-MR, CNRM-CM5, BCC-CSM1-1 and IPSL-CM5A-LR show a spread in temperature increase for the RCP2.6 scenario ranging from 0.7 K to about 1.8 K.

3.2 Effective climate sensitivity (ECS) and transient climate response (TCR)

The effective climate sensitivity (ECS) is an important metric to assess the future warming of the climate system. It is defined as the change in global mean near-surface air temperature as a result of a doubling of the atmospheric CO$_2$ concentration compared to pre-industrial conditions after the climate system has reached a new equilibrium (Gregory et al., 2004). Climate models of the CMIP5 model ensemble simulated an ECS ranging between 2.1 and 4.7 K (Flato et al., 2013). Using all available evidence of that time, IPCC AR5 assessed a “likely” range of ECS between 1.5 and 4.5 K in 2013 (IPCC, 2013). *recipe_ecs.yml* uses a regression method proposed by Gregory et al. (2004) to calculate ECS. Using the total radiative forcing F caused by the doubling of atmospheric CO_2 concentration and the climate feedback parameter λ, ECS is defined as $ECS = F / \lambda$. Both of these variables can be assessed by linear regression of the equation for radiative balance $N = F - \lambda \Delta T$, where N is the net radiation flux at the top of the atmosphere (TOA) and ΔT the global mean near-surface air temperature change. N and ΔT are both given as global and annual mean differences between the abrupt four times CO_2 simulation and the linear regression of the pre-industrial control run. Figure 3~~Figure 3~~ illustrates this regression for the CMIP5 multi-model mean. Moreover, it shows that the assumption of a linear climate feedback parameter is only an approximation. Using only the first 20 years (last 130 years) instead of all 150 years of the abrupt four times CO_2 simulations results in a stronger (weaker) feedback, which again leads to a lower (higher) ECS. This demonstrates the different response of the climate system at different timescales, i.e. non-linear feedback processes. This diagnostic requires the input variables near-surface air temperature (tas), TOA incoming shortwave radiation (rsdt), TOA outgoing shortwave radiation (rsut) and TOA outgoing longwave radiation (rlut) from abrupt4xCO_2 (quadrupling of CO_2 compared to pre-industrial conditions) and piControl (pre-industrial control) simulations.

Figure 9.42a of Flato et al. (2013) shows the globally averaged mean near-surface air temperature (GMSAT) for the historical period 1961-1990 plotted vs. ECS of several CMIP5 models. The latter quantity can be calculated by a regression method based on Gregory et al. (2004) as outlined above. A similar figure produced with *recipe_flato13ipcc.yml* implemented in ESMValTool v2.0 shows that there are no distinctive correlations between the historical surface temperatures and the ECS, which suggests that the ECS is not very sensitive to errors in the current climate in contrast to other sources of uncertainty (Figure 4~~Figure 4~~).

The transient climate response (TCR) is defined as the global and annual mean near-surface air temperature anomaly in the 1pctCO2 simulation (1% increase in CO_2 per year) for a 20-year period centered at the time of CO_2 doubling, i.e. using the years 61 to 80 after the start of the simulation. The temperature anomalies are calculated by subtracting a linear fit to the piControl run for all 140 years from the 1pctCO2 experiment prior to the TCR calculation (Gregory and Forster, 2008). Figure 5~~Figure 5~~ shows (a) a time series of the 1pctCO2 near-surface temperature anomalies from MIROC-ESM used to obtain TCR and (b) TCR values for different CMIP5 models calculated with *recipe_tcr.yml*.

3.3 Emergent constraints

An emergent constraint utilizes an ensemble of ESMs together with observational data to constrain a simulated future Earth system feedback. A prerequisite for an emergent constraint is a robust relationship between, for example, changes occurring on seasonal or interannual time scales and changes found in ESM simulations of anthropogenically-forced climate change (Eyring et al., 2019). If such a relationship can be explained by a plausible physical mechanism, an observational constraint of multi-model projections of quantities that cannot be observed directly might be possible. Such a non-observable quantity is, for instance, ECS. The technique of emergent constraints offers the possibility to reduce uncertainties in climate projections and can help guiding model development by highlighting processes that are crucial to explaining the magnitude and spread of the modeled future climate change. Emergent constraints can also help pointing out the need for more and/or more reliable observations.

We would like to note that a limitation of the emergent constraints as currently implemented into the ESMValTool is that model interdependency, as in the original studies, is not explicitly taken into account. As some modeling groups share model components or code the models are not all independent. Duplicated code as well as identical forcing and validation data in multiple models is expected to lead to an overestimation of the sample size of a model ensemble and may result in spurious correlations (Sanderson et al., 2015). As a possible approach future implementations of these emergent constraints could, for example, apply a model weighting based on a model's interdependence (e.g. Knutti et al. (2017)) or simply reduce the ensemble size taking into account models only that are above a given yet to be defined interdependence score.

Table 2~~Table 2~~ summarizes the emergent constraints that have been implemented in ESMValTool (v2.0) including the observational datasets used and are described in the following.

3.3.1 Emergent constraints on effective climate sensitivity

recipe_ecs_scatter.yml calculates five emergent constraints for ECS (see Table 2~~Table 2~~). These are briefly described in the Sections 3.3.1.1 to 3.3.1.5. The ECS values from the models are pre-calculated with *recipe_ecs.yml* (see Section 3.2) or can be taken from literature. The diagnostic calculates ECS vs. selected constraining parameters such as, for instance, the climatological Hadley cell extent from models, and fits a linear regression line to the data. If available, the observational uncertainty of a given observational dataset can be estimated. For this, the standard error of the observations is subtracted or added from or to the means before calculating the observational value (estimated minimum or maximum, respectively). In addition to the scatter plots of ECS vs. constraining parameter calculated by the diagnostic, the diagnostic also outputs the 25% / 75% confidence intervals of the regression (i.e. uncertainty of the fit) and the 25% / 75% prediction intervals of the regression (i.e. measure for the quality of the linear fit). By definition, 50% of all model data points are within the 25% / 75% prediction interval of the regression line. Examples of the different scatterplots that can be created by *recipe_ecs_scatter.yml* are shown in Figure 6~~Figure 6~~. It should be noted that because a different set of CMIP5 models might be used in the figures compared to the originally published emergent constraints, the figures could show some deviations to the ones published in literature. While the emergent constraints shown in Figure 6~~Figure 6~~a,c,d,e suggest ECS values in the upper range of the values given in IPCC AR5 ((IPCC) (2007), 1.5 to 4.5 K), the emergent constraint shown in Figure 6~~Figure 6~~b suggests an ECS value in the lower range of the IPCC AR5 values.

In addition to these five emergent constraints, *recipe_cox18nature.yml* implements an emergent constraint for ECS based on global temperature variability (Section 3.3.1.6), *recipe_ecs_multivariate_constraint_cmip5.yml* an emergent constraint based on the difference between tropical and mid-latitude cloud fraction (Section 3.3.1.7).

3.3.1.1 Covariance of shortwave cloud reflection

This emergent constraint uses the models' correlation ~~of the covariance~~ of tropical low-level cloud (TLC) reflection with the underlying SST to constrain ECS (Brient and Schneider, 2016). The definition and calculation of the individual terms follows Brient and Schneider (2016): TLC regions are defined as the 25% ocean areas between 30°S and 30°N with the lowest 500-hPa relative humidity. TLC reflection is calculated as the ratio of top of the atmosphere shortwave cloud radiative forcing and insolation, both averaged over the TLC region. This is then used to calculate the regression coefficients of deseasonalized variations of TLC shortwave reflection and sea surface temperature in % per K used as an emergent constraint. In the example shown in Figure 6~~Figure 6~~a, data from the CMIP5 historical simulations between 1980 and 2005 are used for the models, observational / reanalysis data used in Figure 6~~Figure 6~~ are ERA-Interim (Dee et al., 2011) for relative humidity, HadISST (Rayner et al., 2003) for sea surface temperatures, and CERES-EBAF (Ed2.7) (Loeb et al., 2012) for top of the atmosphere radiative fluxes.

3.3.1.2 Climatological Hadley cell extent

Lipat et al. (2017) found that the climatological mean Hadley cell (HC) edge latitude from CMIP5 models correlates with ECS. The HC edge latitude is calculated from first two grid cells from the equator going south where the zonal average 500-hPa mass stream function changes sign from negative to positive (downward branch of the HC). The mass stream function is calculated from climatological December-January-February (DJF) means of the meridional wind fields. The correlation of the climatological HC extent with ECS found in CMIP5 models is explained by observations that show a correlation of variability in mid-latitude clouds and cloud radiative effects with poleward HC expansion (Lipat et al., 2017). For the example shown in Figure 6~~Figure 6~~b, CMIP5 data from historical simulations and ERA-Interim (Dee et al., 2011) as reference dataset for the years 1980-2005 are used.

3.3.1.3 Lower tropospheric mixing index

Following Sherwood et al. (2014), the lower tropospheric mixing index (LTMI) can be used to constrain ECS and is calculated as the sum of small-scale mixing S and the large-scale component of mixing D. S is calculated from relative humidity (RH) and temperature (T) differences between 700 and 850 hPa and averaged over a tropical region between 30°S and 30°N defined by the upper quartile of the annual mean 500-hPa ascent rate within ascending regions: $S = (\Delta RH_{700\text{-}850}/100\% - \Delta T_{700\text{-}850}/9K) / 2$. The large-scale component of mixing is the ratio of shallow to deep overturning: $D = \langle \Delta H(\Delta)H(-\omega_1)\rangle / \langle -\omega_2 H(-\omega_2)\rangle$ with ω_1 the average of the vertical velocity at 850 and 700 hPa, ω_2 the average of the vertical velocity at 600, 500, and 400 hPa, H the step function, and $\langle\ldots\rangle$ the average over the tropical ocean region 160°W-30°E, 30°S-30°N. The lower tropospheric mixing index is calculated as LTMI = S + D. Sherwood et al. (2014) explain the correlation between LTMI and ECS in CMIP3 and CMIP5 models by convective mixing between the lower and middle tropical troposphere dehydrating low-level cloud layers at an increasing rate as climate warms. They argue that this rate of increase depends on initial mixing strength, which links the mixing to clouds feedbacks and thus ECS. Figure 6~~Figure 6~~c shows an example of this emergent constraint applied to CMIP5 historical simulations using ERA-Interim data (Dee et al., 2011) as reference data. All datasets in this example cover the time period 1980-2005.

3.3.1.4 Southern ITCZ index

The southern ITCZ index (Bellucci et al., 2010; Hirota et al., 2011) is defined as the climatological annual mean precipitation bias averaged over the south-eastern Pacific (30°S-0°, 150°W-100°W) given in mm day^{-1}. The southern ITCZ index is used to quantify the double-ITCZ bias in CMIP3 and CMIP5 models and has been found to correlate with ECS (Tian, 2015). In the example shown in Figure 6~~Figure 6~~d, the ITCZ index has been calculated from CMIP5 historical model simulations averaged over the years 1980-2005. TRMM (Huffman et al., 2007) satellite data (v7) averaged over the years 1998-2013 have been used as observational reference.

3.3.1.5 Tropical mid-tropospheric humidity asymmetry index

The strong link found in CMIP3 and CMIP5 models between the double-ITCZ bias and simulated moisture, precipitation, clouds, and large-scale circulation allows the double-ITCZ bias and thus ECS to also be related to mid-tropospheric humidity over the tropical Pacific (Tian, 2015). As shown by Tian (2015), spatial patterns of mid-tropospheric humidity and precipitation are similar as both are related to the ITCZ. This allows defining a tropical mid-tropospheric humidity asymmetry index to quantify the double-ITCZ bias in models and consequently constrain ECS. This index is defined as relative bias in simulated annual mean 500-hPa specific humidity compared with observations ((model – observation) / observation * 100%) averaged over the Southern Hemisphere (SH) tropical Pacific (30°S-0°, 120°E-80°W) minus the bias averaged over the Northern Hemisphere (NH) tropical Pacific (20°N-0°, 120°E-80°W) (Tian, 2015). The example for the tropical mid-tropospheric humidity asymmetry index shown in Figure 6~~Figure 6~~e is calculated from CMIP5 historical runs averaged over the years 1980-2005 and AIRS (v5) satellite data (Susskind et al., 2006) averaged over the years 2003-2010 as observational reference data.

3.3.1.6 Global temperature variability

Cox et al. (2018) propose an emergent constraint for the ECS using global temperature variability. The latter is defined by a metric ψ which can be calculated from the global temperature variance (in time) σ_T and the one-year-lag autocorrelation of the global temperature α_{1T} by

$$\psi = \frac{\sigma_T}{\sqrt{-\ln(\alpha_{1T})}}.$$

Using the simple "Hasselmann model" (Hasselmann, 1976), Cox et al. (2018) showed that ψ is linearly correlated with ECS in CMIP5 data. Since calculation of ψ only depends on the temporal evolution of the global surface temperature, there are many observational datasets available. In the original publication, data from HadCRUT4 (Morice et al., 2012) are used to construct the emergent relationship. In the ESMValTool, this is reproduced by *recipe_cox18nature.yml*, which only needs the two variables historical near-surface air temperature (tas) and ECS (see Section 3.2). The emergent relationship between ECS and ψ is shown in Figure 7~~Figure 7~~ including means and confidence intervals. The constrained range of ECS based on this plot is 2.2 K to 3.4 K with a 66% confidence interval, similar to Cox et al. (2018).

3.3.1.7 Difference between tropical and mid-latitude cloud fraction

Volodin (2008) proposes an emergent constraint for ECS based on the distribution of clouds in global climate models. The study finds that models with high climate sensitivity show a higher total cloud cover over the southern mid-latitudes and a lower total cloud cover over the tropics than the multi-model average. Thus, the difference in tropical total cloud cover (between 28°S and 28°N) and the SH mid-latitude total cloud cover (between 56°S and 36°S) is negatively correlated with ECS. The original publication uses the CMIP3 ensemble and the ISCCP-D2 dataset (Rossow and Schiffer, 1991) as observational reference, but the relationship also holds when using CMIP5 models. In the ESMValTool, this emergent constraint for ECS can be produced with *recipe_ecs_multivariate_constraint_cmip5.yml*, which uses CMIP5 historical runs averaged between 1980 and 2000 (Figure 8~~Figure 8~~). The observed values are based on ISCCP-D2 data and are taken from Volodin (2008).

3.3.2 Emergent constraints on the carbon cycle

Uncertainties in projections of future temperature using ESMs are high, in a large part due to uncertainties of emissions and feedbacks. Within the carbon-cycle, feedbacks are usually split into the carbon cycle – climate feedback γ, which quantifies carbon to climate change, and the carbon cycle – CO_2 concentration feedback β, which is the carbon sensitivity to atmospheric CO_2 (Friedlingstein et al., 2006). γ is a positive feedback as climate warming reduces~~ing~~ the efficiency of CO_2 absorption by the land and ocean, leading to more of the emitted carbon staying in the atmosphere which in turn leads to additional warming. In con~~s~~trast, β is a negative feedback because of the so-called CO_2 fertilization effect, where plants take up a higher amount of CO_2 for photosynthesis with increasing atmospheric CO_2 concentrations. Efforts have been made to reduce the uncertainties of these two carbon cycle feedback parameters.

Wenzel et al. (2014) employed the emergent constraint described by Cox et al. (2013) for the long-term sensitivity of tropical land carbon storage to climate warming (γ_{LT}) to the interannual sensitivity of atmospheric CO_2 to interannual tropical temperature variability (γ_{IAV}) in CMIP5 models. The analysis from this paper can be reproduced using *recipe_wenzel14jgr.yml* with the emergent relationship being able to reduce the range of projected γ_{LT} (Figure 9~~Figure 9~~). Input variables include net primary productivity (nbp), surface temperature (tas), gas exchange flux of CO_2 into the ocean (fgco2) from the experiment 1pctCO2, nbp, fgco2, tas from the emission driven historical simulations (esmHistorical), as well as nbp from the esmFixClim1 (carbon cycle sees CO_2 concentration increase, but radiation doesn't) simulations. The different simulations are included in γ_{IAV}, which is estimated from both, the 1pctCO2 experiment as well as the esmHistorical simulation, and then compared in the paper. The default observational datasets are NCEP reanalysis (Kalnay et al., 1996) for the surface temperature and the global carbon project (GCP; Le Quere et al. (2015)) for the carbon fluxes.

Wenzel et al. (2016a) developed an emergent constraint for β on land in the extratropics and northern mid-latitudes constraining the projected land photosynthesis with changes in the seasonal cycle of atmospheric CO_2. The figures from this paper can be reproduced with *recipe_wenzel16nat.yml*, with Figure 10~~Figure 10~~ showing the emergent constraint reproduced with the ESMValTool. The unconstrained CO_2 fertilization effect lies at 40 ± 20%, which can be narrowed down to 37 ± 9% in high-latitudes and 32 ± 9% in the extratropics with this emergent constraint. Input variables from the models needed to run this recipe is gross primary productivity (gpp) in the esmFixClim1 simulations, as well as the atmospheric CO_2 concentration (co2) from emission driven historical simulations. Observations used are the atmospheric CO_2 concentrations at Point Barrow (BRW; 156.6°W, 71.3°N), Alaska and Cape Kumukahi, Hawaii (KMK; 155.6°W, 19.5°N) (NOAA, 2018).

3.3.3 Emergent constraints on the year of disappearance of September Arctic sea ice

This sea ice diagnostic produces scatterplots of (a) mean of and (b) trend in historical Arctic September sea ice extent (SSIE) vs. first year of disappearance (YOD). Here, YOD is defined as the first of five consecutive years in which the Arctic SSIE drops below one million km² (Wang and Overland, 2009). Sea ice extent is defined in the diagnostic as the total area of all grid cells in which the sea ice concentration is 15% or larger, Arctic is defined as the region north of 60°N. The annual minimum Arctic sea ice extent typically occurs in September. For this reason, September mean sea ice quantities are commonly used in literature for analyses of the timing of an ice-free Arctic (e.g., Massonnet et al. (2012); Sigmond et al. (2018)). The two scatterplots (Figure 11~~Figure 11~~a) and (Figure 11~~Figure 11~~b) are similar to figures 12.31 a/c of Collins et al. (2013), respectively. In addition, the diagnostic produces a scatterplot of mean SSIE vs. trend in historical SSIE, similar to figure 2 of Massonnet et al. (2012). In the example shown in Figure 11~~Figure 11~~, HadISST data (Rayner et al., 2003) over the time period 1960-2005 have been used as reference dataset for comparison with CMIP5 results. The figure shows that while the individual models spread widely around the observed mean Arctic SSIE, most of the CMIP5 models tend to underestimate the trend in Arctic SSIE observed over the period 1960-2005.

3.3.4 Emergent constraints on the snow-albedo effect

The recipe *recipe_snowalbedo.yml* computes springtime snow-albedo feedback values in climate change vs. springtime values in the seasonal cycle in transient climate change experiments following Hall and Qu (2006). The strength of the snow-albedo effect is quantified by the variation in net incoming shortwave radiation (Q) with surface air temperature (T_s) due to changes in surface albedo α_s:

$$\left(\frac{\partial Q}{\partial T_s}\right) = -I_t \cdot \frac{\partial \alpha_p}{\partial \alpha_s} \cdot \frac{\Delta \alpha_s}{\Delta T_s}$$

Here, I_t is the constant incoming solar radiation at the top of the atmosphere, α_p the planetary albedo. The diagnostic produces scatterplots of simulated springtime $\Delta\alpha_s$ / ΔT_s values in climate change (ordinate) vs. simulated springtime $\Delta\alpha_s$ / ΔT_s values in the seasonal cycle (abscissa). These values are calculated as follows: (ordinate values) the change in April α_s (future projection - historical) averaged over NH land masses poleward of 30°N is divided by the change in April T_s (future projection - historical) averaged over the same region. The change in α_s (or T_s) is defined as the difference between 22nd century mean α_s (T_s) and 20th-century-mean α_s. Values of α_s are weighted by April incoming insolation (I_t) prior to averaging.

~~(Abscissa values) t~~The seasonal cycle $\Delta\alpha_s$ / ΔT_s values (abscissa values), based on 20th century climatological means, are calculated by dividing the difference between April and May α_s (averaged over NH continents poleward of 30°N) by the difference between April and May T_s averaged over the same area. Values of α_s are weighted by April incoming insolation prior to averaging.

Figure 12~~Figure 12~~ shows an example calculated from CMIP5 historical (1901-2000) and Representative Concentration Pathways 4.5 (RCP4.5, 2101-2200) experiments for 12 different models. The seasonal cycle values used as reference (vertical gray line) are calculated from third generation of ISCCP radiative fluxes (ISCCP-FH, Young et al. (2018)) and near-surface air temperature from ERA-Interim (Dee et al., 2011) for the years 1984-2000. While data from ISCCP-FH data suggest that CMIP5 models tend to underestimate springtime snow-albedo effect values in climate change, using the second generation of ISCCP radiative fluxes (ISCCP-FD, Zhang et al. (2004), not shown) as in figure 9.45a of Flato et al. (2013) suggest that the CMIP5 models under- and overestimate springtime snow-albedo effect almost equally.

3.3.5 Emergent constraints on the hydrological cycle

The recipes *recipe_deangelis2015nat.yml* and *recipe_li2017natcc.yml* newly developed for v2.0 reproduce the analysis from DeAngelis et al. (2015) and Li et al. (2017), respectively. DeAngelis et al. (2015) constrain the hydrologic cycle intensification with observed radiative fluxes and water vapor data. The recipe *recipe_deangelis2015nat.yml* reproduces their figures 1b (Figure 13~~Figure 13~~a) to 4 (Figure 13~~Figure 13~~b) as well as their extended data figures 1 and 2. Here,~~So far~~ the analysis is shown~~available~~ for 17~~21~~ CMIP5 models and includes monthly mean total precipitable water on a 1° x 1°~~ degree~~ grid from RSS (Remote Sensing System) Version-7 microwave radiometer data (Wentz et al., 2007) and ERA-Interim reanalysis (Dee et al., 2011), as well as radiative fluxes from the dataset Clouds and the Earth's Radiant Energy System Energy Balance and Filled (CERES-EBAF, Kato et al. (2013); Loeb et al. (2009)). Figure 13~~Figure 13~~a shows that energy sources and sinks readjust in reply to an increase in greenhouse gases, leading to a decrease in the sensible heat flux and an increase in the other fluxes; Figure 13~~Figure 13~~b shows that results from parameterization schemes using pseudo-k-distributions with more than 20 exponential terms representing water vapor absorption and correlated-k-distributions agree better with the observations than the other schemes.

Li et al. (2017) relate the future Indian summer monsoon projections to the present-day precipitation over the tropical western Pacific. With this relationship they can correct the projected rainfall for models with too strong negative cloud–radiation feedback on sea surface temperature. The corrected values (see Figure 14~~Figure 14~~) do not show an increase in rainfall over the whole ISM region under greenhouse warming and are expected to be more robust than the uncorrected projection (Li et al., 2017). The *recipe_li2017natcc.yml* reproduces their figures 1 and 2 for an ensemble of 22 CMIP5 models (Figure 14~~Figure 14~~) and their figure 1a for each of the individual models and the multi-model mean.

3.4 Climate model projections

In addition to the emergent constraints described in the previous section, ESMValTool v2.0 also includes new diagnostics specifically designed to analyze future climate projections from ESMs. This includes diagnostics using the multiple diagnostic ensemble regression used to constrain the future position of the austral jet, a “toy model” to allow for investigating the effect of observational uncertainty on model evaluation, diagnostics for reproducing selected figures from the climate projection chapter in IPCC AR5 (Collins et al., 2013) and for analyzing future sea ice quantities. All of these new diagnostics in ESMValTool v2.0 are briefly described in the following sections.

3.4.1 MDER to constrain future austral jet position

The position of the austral jet stream is poorly modeled by CMIP5 models with a latitude range of 10° within the ensemble and a mean bias towards the equator. The *recipe_wenzel16jclim.yml* reproduces the study of Wenzel et al. (2016b) who used a process-oriented multiple diagnostic ensemble regression (MDER) to constrain the future jet position in the RCP4.5 scenario. MDER uses a stepwise regression scheme to identify the most relevant present-day diagnostics from a list of diagnostics provided as an input and links those to future projections via a multivariate linear regression scheme. With the diagnostics selected by MDER, the future quantity (in this case the austral jet position) can be constrained with suitable observationally based data (here: ERA-Interim (Dee et al., 2011)), following the same basic idea as emergent constraints (see also section 3.3). Using this approach, the future jet position from CMIP5 models is bias-corrected about 1.5° southwards compared to the unweighted multi-model mean (Figure 15~~Figure 15~~).

3.4.2 Toy model

Synthetic datasets generated from “toy models” have been used in the literature for assessing the effectiveness of multi-model combination strategies and for estimating the effect of observational uncertainties on the correlation between forecasts and observational datasets (Massonnet et al., 2016). The Toy model recipe implemented into ESMValTool v2.0 is based on the approach presented in Weigel et al. (2008) for simulating single-model ensembles from a Gaussian distribution, where the number of members and the standard deviation of the error are defined by the user. Following Weigel et al. (2008), the recipe takes as input a set of observations, y_1, y_2, …, y_N, and for each observation y_i, M synthetic members x are generated from:

$$x_{i,m} = \alpha y_i + \epsilon_\beta + \epsilon_{i,m}$$

where $y \sim N($~~θ~~$\mu,1)$, $\epsilon_\beta \sim N(0,\beta)$ and $\epsilon_1,\ldots,\epsilon_M \sim N(0,\sqrt{(1-\alpha^2-\beta^2)})$ with the notation $N(\mu,\sigma)$ referring to a random number drawn from a normal distribution with mean μ and standard deviation σ. The simulated value x_m is obtained by multiplying y by α, the predictability of the observation, which is set to 1 in this instance, and by adding a vector of perturbations ϵ~~$_{i,}$~~$_m$ and the scalar perturbation ϵ_β. The simulated values have the following properties:

1) The simulated values $x_{i,1}$ have the same climatology as the observations.
2) The mean correlation between the simulations $x_{i,1},\ldots, x_{i,M}$ and observation y_i is determined by α (see toy model properties described in Weigel et al. (2008)).
3) The parameter β describes the model under-dispersion, where β = 0 corresponds to the case where the synthetic ensemble is well dispersed and covers the full range of uncertainties for a given correlation α. The under-dispersion increases with β being limited to the range $0 \leq \beta \leq \sqrt{(1-\alpha^2)}$.

Parameter β is introduced to control the dispersion. For well-dispersed ensembles, skill is independent of the number of simulations involved, while for overconfident model ensembles, skill grows with the ensemble size. Given that β accounts for the dispersion, this approach leads α to represent a measure of predictability (Weigel et al., 2008).

This toy model is based on very simplifying assumptions: (1) normality and stationarity, the climatology and the ensemble distributions are assumed to be stationary and normally distributed; (2) well-calibrated model climatology, each ensemble member has the same climatology as the observations; (3) stationary skill, spread and correlation do not vary from sample to sample; (4) predictable signal and observational errors, requires the signal to be given by αx, and therefore it is determined by the verifying observation (Weigel et al., 2008).

~~Here, t~~The predictability α is 1 since we are only interested in generating synthetic observations. Thus, the user only needs to define the standard deviation of the error. This term can be based on the observational uncertainty when available (e.g. as provided with the European Space Agency's Climate Change Initiative (ESA CCI) SST dataset; Merchant et al. (2014a); Merchant et al. (2014b)) or estimated by the user, e.g. by estimating the standard deviation between different observational reference datasets (Bellprat et al., 2017).

We would like to note that in addition to the observational uncertainty itself, also spatio-temporal representativeness of observations plays an important role when evaluating models. Schutgens et al. (2017) showed that such representation errors remain even after spatial and temporal averaging and may be larger than typical measurement errors. In addition, also the calculation method of a quantity to be compared with observations can play an important role. This is, for example, the case when comparing satellite retrievals with model quantities that are not derived the same way. Application of satellite simulators such as the Cloud Feedback Model Intercomparison Project (CFMIP) Observation Simulator Package (COSP; Bodas-Salcedo et al. (2011)) can help to reduce such uncertainties in model evaluation. Both of these aspects are not covered by the toy model, that only provides an estimate for the observational uncertainty itself.

~~-~~For further discussion of this synthetic value generator, its general application to forecasts and its limitations, see Weigel et al. (2008). The recipe *recipe_toymodel.yml* writes a netCDF file containing the synthetic observations. Due to the sampling of the perturbations from a Gaussian distribution, running the recipe multiple times, with the same observation dataset and input parameters, will result in different outputs (Figure 16~~Figure 16~~).

3.4.3 Climate projection chapter of IPCC WGI AR5

The *recipe_collins13ipcc.yml* reproduces a subset of the figures from the long-term climate change projections chapter of the IPCC AR5 (Chapter 12, Collins et al. (2013)). This new recipe in version 2.0 allows for reproduction of selected figures from AR5 to show changes between historical and future projections over the available CMIP models. It will also allow a faster analysis of the CMIP6 climate projections that are part of the Scenario Model Intercomparison Project (ScenarioMIP, O'Neill et al. (2016)). The recipe includes figures such as time series from historical periods to projections (including spread among models, see Figure 17~~Figure 17~~), horizontal maps for individual models as well as multi-model means (including stippling ~~and hatching~~ to indicate large changes with high model agreement~~significant changes~~ and hatching to indicate areas with a small signal or low agreement of models~~where models do not agree~~, see Figure 18~~Figure 18~~), and vertical zonal mean plots (also including stippling and hatching to indicate significant changes). The example shown in Figure 18~~Figure 18~~ shows where the CMIP5 models project an increase in precipitation and where they project a decrease. This example also shows quite large regions where the projections are still uncertain, i.e. the multi-model mean signal is smaller than one standard deviation of the natural variability estimated from preindustrial control simulations (hatching).

Most diagnostics scripts are set up in a generic way, so that in principle they can be used for any variable from the CMIP archive. The scripts have been tested for the variables indicated in Table 1~~Table 1~~. To be able to determine if a change signal is larger than natural variability the natural variability is calculated from the piControl runs, other than that the recipe uses historical and RCP runs. All diagnostics in this recipe with the exception of the emergent constraints on the year of disappearance of September Arctic sea ice (Section 3.3.3~~3.3.4~~) do not use observations.

3.4.4 Sea ice

The sea ice diagnostics included in the ESMValTool (*recipe_seaice.yml*) have been extended with three new diagnostics. The first new diagnostic *seaice_trends.ncl* calculates the trend in sea ice extent or sea ice area from each model and reference observation(s) or reanalysis data that are given in the recipe. The diagnostic produces histogram plots of the trend distributions from all models and adds the reference datasets (here: HadISST, Rayner et al. (2003)) as colored vertical lines. The user can specify the region (Arctic or Antarctic) and the month of the year for which sea ice area/extent is calculated. The trends are calculated over the full period specified in the recipe and the resulting plots are similar to Flato et al. (2013) Figures 9.24 c/d. The example plot (Figure 19~~Figure 19~~) shows that the majority of CMIP5 models slightly underestimate the observed trend in summer sea ice extent over the time period 1960-2005.

The second new diagnostic *seaice_yod.ncl* calculates the year of near-disappearance of Arctic sea ice. The diagnostic creates a time series plot of September Arctic sea ice extent for each model given in the recipe and adds three multi-model statistics: mean, standard deviation and YOD. It optionally reads a list of pre-calculated model weights and adds the weighted multi-model mean time series including weighted multi-model standard deviation to the plot (see for example figure 7 of Senftleben et al. (2020)). The example in Figure 20~~Figure 20~~ shows that there is a large spread in simulated sea ice extent among the CMIP5 models with individual models simulating a summer sea ice extent below 1 million km^2 already around the year 2025 while other models are still well above this threshold in 2100.

The third new diagnostic *seaice_ecs.ncl* calculates emergent constraints for YOD using mean or trend in sea ice extent. The diagnostic produces scatter plots of different historical and future sea ice metrics, similar to figure 2 of Massonnet et al. (2012) and figures 12.31 a/c of Collins et al. (2013) (see Section 3.3.3~~3.3.4~~ for details).

4 Summary

~~This paper is part of a series of four articles describing the new features and diagnostics of the Earth System Model Evaluation Tool v2.0. Version 2.0 is a major upgrade from the last release v1.1.0 (Eyring et al., 2016b; Lauer et al., 2017). Besides many technical improvements including greatly improved performance and user-friendliness (Righi et al., 2020), version 2.0 includes new large-scale diagnostics for evaluation of Earth system models (Eyring et al., in review) and diagnostics for extreme events, regional model and impact evaluation and analysis of ESM results (Weigel et al., in prep.).~~ In this article, ~~newly implemented~~ diagnostics and metrics newly implemented into the Earth System Model Evaluation Tool v2.0 to analyze projections from ESMs and emergent constraints for climate-relevant parameters including effective climate sensitivity, snow-albedo effect, climate-carbon cycle feedback, hydrologic cycle intensification, future Indian summer monsoon precipitation, land photosynthesis and year of disappearance of summer Arctic sea ice are described and illustrated with examples using CMIP5 data~~.~~

The implemented multi-model products ~~(*recipe_multimodel_products.yml*)~~ allow for an easy and quick overview of the multi-model ensemble mean and the inter-model agreement in the sign of the multi-model mean anomaly for a given variable, geographical region, season and time period. In addition to maps showing the anomalies and their inter-model agreement, the results are also given as anomaly time series showing each individual model and the multi-model ensemble mean, which can be used to estimate the inter-model spread.

~~Effective climate sensitivity and transient climate response can be calculated for a model ensemble with *recipe_ecs.yml* and *recipe_tcr.yml*, respectively. Both,~~ ECS and TCR~~,~~ are climate metrics that can be used to estimate and compare the sensitivity of~~the~~ simulated near-surface temperature from individual models to increased atmospheric CO_2 concentrations. With these metrics included in the ESMValTool, it is easily possible to group the models in high- and low-sensitivity models for further analysis.

Emergent constraints offer the possibility to use an ensemble of ESMs together with observations in order to constrain non-observable parameters such as simulated future Earth system feedbacks. Seven emergent constraints are available in ESMValTool v2.0 for ECS~~(*recipe_ecs_scatter.yml*, *recipe_cox18nature.yml* and *recipe_ecs_multivariate_constraint_cmip5.yml*)~~: (1) covariance of shortwave cloud reflection using the models' correlation of the covariance of tropical low-level cloud reflection with the underlying SST (Brient and Schneider, 2016); and (2) latitude of the climatological mean Hadley cell edge (Lipat et al., 2017); (3) atmospheric convective mixing calculated as sum of small- and large-scale component, the lower tropospheric mixing index (Sherwood et al., 2014); (4) bias in climatological annual mean precipitation over the south-eastern Pacific, the southern ITCZ index (Tian, 2015); mid-tropospheric humidity over the tropical Pacific, the tropical mid-tropospheric humidity asymmetry index (Tian, 2015); (6) global temperature variability (Cox et al., 2018); and (7) difference between tropical and mid-latitude cloud fraction (Volodin, 2008). Two emergent constraints on the hydrological cycle are implemented: (1) a constraint on the hydrological cycle intensification that uses observations of radiative fluxes and water vapor (DeAngelis et al., 2015)~~in *recipe_deangelis2015nat.yml*~~; and (2) a constraint on the future Indian summer monsoon using present-day precipitation data over the tropical western Pacific (Li et al., 2017)~~ implemented in *recipe_li2017natcc.yml*~~. Additionally, emergent constraints are available for the carbon cycle: (1) future tropical land carbon storage (Wenzel et al., 2014)~~, *recipe_wenzel14jgr.yml*~~; (2) projected land photosynthesis (Wenzel et al., 2016a)~~, *recipe_wenzel16nat.yml*~~. Also implemented are emergent constraints for the year of disappearance of September Arctic sea ice (Massonnet et al., 2012)~~ in *recipe_seaice.yml*~~ and for the snow-albedo effect (Hall and Qu, 2006)~~ (*recipe_snowalbedo.yml*)~~.

Various new diagnostics are available specifically for analysis of climate model projections. The multiple diagnostic ensemble regression (MDER) method has been implemented to constrain the projected position of the austral jet following Wenzel et al. (2016b). The method uses a stepwise regression to identify the most relevant diagnostics (calculated with present-day data) that are linked to projections of a quantity via a multivariate linear regression scheme. Observational data can then be used to constrain the projected quantity such as the future austral jet position~~ (*recipe_wenzel16jclim.yml*)~~.

A number of newly implemented diagnostics resembling selected figures from IPCC AR5 chapter 12 (Collins et al., 2013) for analysis of climate model projections are grouped in one recipe~~*recipe_collins13ipcc.yml*~~. The diagnostics include time series and horizontal maps and vertical zonal maps including stippling and hatching to show significant changes between a climate projection scenario and a historical simulation. For the stippling and hatching, results from pre-industrial control runs are used to estimate internal variability of a variable, which is then used to assess whether simulated changes are significant or not. ~~In *recipe_seaice.yml*, d~~Diagnostics to analyze sea ice in climate model simulations are also grouped in one recipe. The new diagnostics include calculation of trends in sea ice area and extent, multi-model estimates for the year of disappearance of sea ice in climate projections, and scatter plots of different historical and future sea ice metrics such as historical trend in sea ice extent vs. YOD. In addition, a "toy model"~~ (*recipe_toymodel.yml*)~~ has been implemented into ESMValTool v2.0 that allows generating synthetic ensemble members from a single dataset (Weigel et al., 2008). When applied to observational data, this can be used to take into account observational uncertainty when comparing the observations with model results. For this, the user needs to specify the standard error of the observations that is provided with some observational datasets or estimated from differences between different observational datasets for the same quantity.

The ESMValTool v2.0 is an open source software tool that has been specifically developed to facilitate evaluation and analysis of Earth system models participating in CMIP. As such, it can process and analyze CMOR compliant model output and observational datasets with the particular aim to provide traceable and reproducible results, well-documented diagnostics and metrics and an efficient workflow allowing to evaluate models in more depth and more rapidly than it was typically possible in previous CMIP phases. The CMOR standard is, however, quite detailed and implemented in a relatively strict way in the ESMValTool in order to ensure data consistency and to minimize the probability of errors in the data processing. Increasing the flexibility of the CMOR check and automatic fixes of small inconsistencies is a currently ongoing activity and should make the data processing smoother, especially for datasets which are not part of CMIP or any CMIP-Endorsed-Model-Intercomparison-Project (MIP). This means that a certain familiarity with these data standards is required in order to use the ESMValTool. Another limitation is that for license issues, observations cannot be distributed together with the software package. New users are required to download and process observational datasets before being able to use the tool or to have access to a computing center where observational data for the ESMValTool (i.e. cmorized) are already available. We are currently working on automating this process to facilitate the data retrieval and cmorization process.

~~ESMValTool v2.0 has been specifically developed in order to analyze and evaluate the latest generation of CMIP model results.~~ The new ESMValTool v~~ersion~~ 2.0 is now available to the community for evaluation and scientific analyses of CMIP6 data. Thanks to a strong community involvement, the ESMValTool is constantly extended and improved in an effort to make the tool more user friendly, more efficient and a better tool for climate analyses. ~~The ESMValTool development team will continue to improve and extend the tool.~~ The ongoing ESMValTool development and discussions regarding new features can be followed on GitHub at https://github.com/ESMValGroup. Feedback, bug reports and contributions by the scientific community are very welcome at any time.

5 Code availability

ESMValTool v2.0 is released under the Apache License, VERSION 2.0. The latest release of ESMValTool v2.0 is publicly available on Zenodo at https://doi.org/10.5281/zenodo.3401363. The source code of the ESMValCore package, which is installed as a dependency of the ESMValTool v2.0, is also publicly available on Zenodo at https://doi.org/10.5281/zenodo.3387139. ESMValTool and ESMValCore are developed on the GitHub repositories available at https://github.com/ESMValGroup.

6 Data availability

CMIP5 data are available freely and publicly from the Earth System Grid Federation (ESGF). Observations used in the evaluation are detailed in the various sections of the manuscript. The observational datasets are not distributed with the ESMValTool that is restricted to the code as open source software. Observational datasets that are available through the Observations for Model Intercomparisons Project (obs4MIPs, https://esgf-node.llnl.gov/projects/obs4mips/) can be downloaded freely from the ESGF and ~~used~~ directly used in~~with~~ the ESMValTool. For all other observational datasets, the ESMValTool provides a collection of scripts (NCL and Python) with exact downloading and processing instructions to recreate the datasets used in this publication.

Author contribution

AL and VE coordinated the ESMValTool v2.0 diagnostic effort and led the writing of the paper. MR helped coordinating the diagnostic implementation and testing in ESMValTool v2.0. All other authors contributed individual diagnostics to this release. All authors contributed to the text.

Competing interests

The authors declare that they have no conflict of interest.

Acknowledgements

The development of ESMValTool (v2.0) is supported by several projects. The diagnostic development of ESMValTool v2.0 for this paper was supported by different projects with different scientific focus, in particular by (1) European Union's Horizon 2020 Framework Programme for Research and Innovation "Coordinated Research in Earth Systems and Climate: Experiments, kNowledge, Dissemination and Outreach (CRESCENDO)" project under Grant Agreement No. 641816, (2) European Union's Horizon 2020 project "Climate-Carbon Interactions in the Coming Century" (4C) under Grant Agreement No. 821003, (~~2~~3)

Copernicus Climate Change Service (C3S) "Metrics and Access to Global Indices for Climate Projections (C3S-MAGIC)" project, (~~3~~4) Federal Ministry of Education and Research (BMBF) CMIP6-DICAD project, (5~~4~~) ESA Climate Change Initiative Climate Model User Group (ESA CCI CMUG), and (6~~5~~) Helmholtz Society project "Advanced Earth System Model Evaluation for CMIP (EVal4CMIP)". In addition, we received technical support on the ESMValTool v2.0 development from the European Union's Horizon 2020 Framework Programme for Research and Innovation "Infrastructure for the European Network for Earth System Modelling (IS-ENES3)" project under Grant Agreement No 824084.

We acknowledge the World Climate Research Program's (WCRP's) Working Group on Coupled Modelling (WGCM), which is responsible for CMIP, and we thank the climate modelling groups for producing and making available their model output. We thank Franziska Winterstein (DLR) for her helpful comments on the manuscript. The computational resources of the Deutsches Klimarechenzentrum (DKRZ, Germany) were essential for developing and testing this new version and are kindly acknowledged.

7 References

(IPCC), I. P. o. C. C.: The Physical Science Basis, Contribution of Working Group I to the Fourth Assessment Report of the Intergovernmental Panel on Climate Change, Cambridge University Press, Cambridge, United Kingdom and New York, NY, USA, 2007.

Adler, R. F., Huffman, G. J., Chang, A., Ferraro, R., Xie, P. P., Janowiak, J., Rudolf, B., Schneider, U., Curtis, S., Bolvin, D., Gruber, A., Susskind, J., Arkin, P., and Nelkin, E.: The version-2 global precipitation climatology project (GPCP) monthly precipitation analysis (1979-present), J Hydrometeorol, 4, 1147-1167, 2003.

Bellprat, O., Massonnet, F., Siegert, S., Prodhomme, C., Macias-Gómez, D., Guemas, V., and Doblas-Reyes, F. J. R. S. o. E.: Uncertainty propagation in observational references to climate model scales, 203, 101-108, 2017.

Bellucci, A., Gualdi, S., and Navarra, A. J. J. o. C.: The double-ITCZ syndrome in coupled general circulation models: the role of large-scale vertical circulation regimes, 23, 1127-1145, 2010.

Bodas-Salcedo, A., Webb, M. J., Bony, S., Chepfer, H., Dufresne, J. L., Klein, S. A., Zhang, Y., Marchand, R., Haynes, J. M., Pincus, R., and John, V. O.: COSP Satellite simulation software for model assessment, B Am Meteorol Soc, 92, 1023-1043, 2011.

Brient, F. and Schneider, T.: Constraints on Climate Sensitivity from Space-Based Measurements of Low-Cloud Reflection, J Climate, 29, 5821-5835, 2016.

Collins, M., Knutti, R., Arblaster, J., Dufresne, J.-L., Fichefet, T., Friedlingstein, P., Gao, X., Gutowski, W. J., Johns, T., Krinner, G., Shongwe, M., Tebaldi, C., Weaver, A. J., and Wehner, M.: Long-term Climate Change: Projections, Commitments and Irreversibility. In: Climate Change 2013: The Physical Science Basis. Contribution of Working Group I to the Fifth Assessment Report of the Intergovernmental Panel on Climate Change, Stocker, T. F., Qin, D., Plattner, G.-K., Tignor, M., Allen, S. K., Boschung, J., Nauels, A., Xia, Y., Bex, V., and Midgley, P. M. (Eds.), Cambridge University Press, Cambridge, United Kingdom and New York, NY, USA, 2013.

Cox, P. M., Huntingford, C., and Williamson, M. S. J. N.: Emergent constraint on equilibrium climate sensitivity from global temperature variability, 553, 319, 2018.

Cox, P. M., Pearson, D., Booth, B. B., Friedlingstein, P., Huntingford, C., Jones, C. D., and Luke, C. M.: Sensitivity of tropical carbon to climate change constrained by carbon dioxide variability, Nature, 494, 341-344, 2013.

DeAngelis, A. M., Qu, X., Zelinka, M. D., and Hall, A.: An observational radiative constraint on hydrologic cycle intensification, Nature, 528, 249, 2015.

Dee, D. P., Uppala, S. M., Simmons, A. J., Berrisford, P., Poli, P., Kobayashi, S., Andrae, U., Balmaseda, M. A., Balsamo, G., Bauer, P., Bechtold, P., Beljaars, A. C. M., van de Berg, L., Bidlot, J., Bormann, N., Delsol, C., Dragani, R., Fuentes, M., Geer, A. J., Haimberger, L., Healy, S. B., Hersbach, H., Holm, E. V., Isaksen, L., Kallberg, P., Kohler, M., Matricardi, M., McNally, A. P., Monge-Sanz, B. M., Morcrette, J. J., Park, B. K., Peubey, C., de Rosnay, P., Tavolato, C., Thepaut, J. N., and Vitart, F.: The ERA-Interim reanalysis: configuration and performance of the data assimilation system, Q J Roy Meteor Soc, 137, 553-597, 2011.

Eyring, V., Bock, L., Lauer, A., Righi, M., Schlund, M., Andela, B., Arnone, E., Bellprat, O., Brötz, B., Caron, L.-P., Carvalhais, N., Cionni, I., Cortesi, N., Crezee, B., Davin, E., Davini, P., Debeire, K., de Mora, L., Deser, C., Docquier, D., Earnshaw, P., Ehbrecht, C., Gier, B. K., Gonzalez-Reviriego, N., Goodman, P., Hagemann, S., Hardiman, S., Hassler, B., Hunter, A., Kadow, C., Kindermann, S., Koirala, S., Koldunov, N., Lejeune, Q., Lembo, V., Lovato, T., Lucarini, V., Massonnet, F., Müller, B., Pandde, A., Pérez-Zanón, N., Phillips, A., Predoi, V., Russell, J., Sellar, A., Serva, F., Stacke, T., Swaminathan, R., Torralba, V., Vegas-Regidor, J., von Hardenberg, J., Weigel, K., and Zimmermann, K.: ESMValTool v2.0 – Extended set of large-scale diagnostics for quasi-operational and comprehensive evaluation of Earth system models in CMIP, Geosci. Model Dev. Discuss., doi: 10.5194/gmd-2019-291, in review. in review.

Eyring, V., Bony, S., Meehl, G. A., Senior, C. A., Stevens, B., Stouffer, R. J., and Taylor, K. E.: Overview of the Coupled Model Intercomparison Project Phase 6 (CMIP6) experimental design and organization, Geosci Model Dev, 9, 1937-1958, 2016a.

Eyring, V., Cox, P. M., Flato, G. M., Gleckler, P. J., Abramowitz, G., Caldwell, P., Collins, W. D., Gier, B. K., Hall, A. D., and Hoffman, F. M. J. N. C. C.: Taking climate model evaluation to the next level, 2019. 1, 2019.

Eyring, V., Righi, M., Lauer, A., Evaldsson, M., Wenzel, S., Jones, C., Anav, A., Andrews, O., Cionni, I., Davin, E. L., Deser, C., Ehbrecht, C., Friedlingstein, P., Gleckler, P., Gottschaldt, K. D., Hagemann, S., Juckes, M., Kindermann, S., Krasting, J., Kunert, D., Levine, R., Loew, A., Makela, J., Martin, G., Mason, E., Phillips, A. S., Read, S., Rio, C., Roehrig, R., Senftleben, D., Sterl, A., van Ulft, L. H., Walton, J., Wang, S. Y., and Williams, K. D.: ESMValTool (v1.0) - a community diagnostic and performance metrics tool for routine evaluation of Earth system models in CMIP, Geosci Model Dev, 9, 1747-1802, 2016b.

Flato, G., Marotzke, J., Abiodun, B., Braconnot, P., Chou, S. C., Collins, W., Cox, P., Driouech, F., Emori, S., Eyring, V., Forest, C., Gleckler, P., Guilyardi, E., Jakob, C., Kattsov, V., Reason, C., and Rummukainen, M.: Evaluation of Climate Models. In: Climate Change 2013: The Physical Science Basis. Contribution of Working Group I to the Fifth Assessment Report of the Intergovernmental Panel on Climate Change, Stocker, T. F., D. Qin, G.-K. Plattner, M. Tignor, S.K. Allen, J. Boschung, A. Nauels, Y. Xia, V. Bex and P.M. Midgley (Ed.), Cambridge University Press, Cambridge, United Kingdom and New York, NY, USA, 2013.

Friedlingstein, P., Cox, P., Betts, R., Bopp, L., Von Bloh, W., Brovkin, V., Cadule, P., Doney, S., Eby, M., Fung, I., Bala, G., John, J., Jones, C., Joos, F., Kato, T., Kawamiya, M., Knorr, W., Lindsay, K., Matthews, H. D., Raddatz, T., Rayner, P., Reick, C., Roeckner, E., Schnitzler, K. G., Schnur, R., Strassmann, K., Weaver, A. J., Yoshikawa, C., and Zeng, N.: Climate-carbon cycle feedback analysis: Results from the (CMIP)-M-4 model intercomparison, J Climate, 19, 3337-3353, 2006.

Gregory, J. M. and Forster, P. M.: Transient climate response estimated from radiative forcing and observed temperature change, J Geophys Res-Atmos, 113, 2008.

Gregory, J. M., Ingram, W., Palmer, M., Jones, G., Stott, P., Thorpe, R., Lowe, J., Johns, T., and Williams, K. J. G. R. L.: A new method for diagnosing radiative forcing and climate sensitivity, 31, 2004.

Hall, A. and Qu, X.: Using the current seasonal cycle to constrain snow albedo feedback in future climate change, Geophysical Research Letters, 33, 2006.

Hasselmann, K.: Stochastic climate models Part I. Theory, Tellus, 28, 473-485, 1976.

Hirota, N., Takayabu, Y. N., Watanabe, M., and Kimoto, M. J. J. o. C.: Precipitation reproducibility over tropical oceans and its relationship to the double ITCZ problem in CMIP3 and MIROC5 climate models, 24, 4859-4873, 2011.

Huffman, G. J., Bolvin, D. T., Nelkin, E. J., Wolff, D. B., Adler, R. F., Gu, G., Hong, Y., Bowman, K. P., and Stocker, E. F. J. J. o. h.: The TRMM multisatellite precipitation analysis (TMPA): Quasi-global, multiyear, combined-sensor precipitation estimates at fine scales, 8, 38-55, 2007.

IPCC: Climate Change 2013: The Physical Science Basis. Contribution of Working Group I to the Fifth Assessment Report of the Intergovernmental Panel on Climate Change, Cambridge University Press, Cambridge, United Kingdom and New York, NY, USA, 2013.

IPCC: Intergovernmental Panel on Climate Change (IPCC), Climate Change 2007: The Physical Science Basis. Contribution of Working Group I to the Fourth Assessment Report of the Intergovernmental Panel on Climate Change, Cambridge, United Kingdom and New York, NY, USA, 2007.

Kalnay, E., Kanamitsu, M., Kistler, R., Collins, W., Deaven, D., Gandin, L., Iredell, M., Saha, S., White, G., Woollen, J., Zhu, Y., Chelliah, M., Ebisuzaki, W., Higgins, W., Janowiak, J., Mo, K. C., Ropelewski, C., Wang, J., Leetmaa, A., Reynolds, R., Jenne, R., and Joseph, D.: The NCEP/NCAR 40-year reanalysis project, B Am Meteorol Soc, 77, 437-471, 1996.

Kato, S., Loeb, N. G., Rose, F. G., Doelling, D. R., Rutan, D. A., Caldwell, T. E., Yu, L. S., and Weller, R. A.: Surface Irradiances Consistent with CERES-Derived Top-of-Atmosphere Shortwave and Longwave Irradiances, J Climate, 26, 2719-2740, 2013.

Knutti, R., Sedlacek, J., Sanderson, B. M., Lorenz, R., Fischer, E. M., and Eyring, V.: A climate model projection weighting scheme accounting for performance and interdependence, Geophys Res Lett, 44, 1909-1918, 2017.

Lauer, A., Eyring, V., Righi, M., Buchwitz, M., Defourny, P., Evaldsson, M., Friedlingstein, P., de Jeu, R., de Leeuw, G., Loew, A., Merchant, C. J., Müller, B., Popp, T., Reuter, M., Sandven, S., Senftleben, D., Stengel, M., Van Roozendael, M., Wenzel, S., and Willén, U.: Benchmarking CMIP5 models with a subset of ESA CCI Phase 2 data using the ESMValTool, Remote Sensing of Environment, doi: 10.1016/j.rse.2017.01.007, 2017. 2017.

Le Quere, C., Moriarty, R., Andrew, R. M., Peters, G. P., Ciais, P., Friedlingstein, P., Jones, S. D., Sitch, S., Tans, P., Arneth, A., Boden, T. A., Bopp, L., Bozec, Y., Canadell, J. G., Chini, L. P., Chevallier, F., Cosca, C. E., Harris, I., Hoppema, M., Houghton, R. A., House, J. I., Jain, A. K., Johannessen, T., Kato, E., Keeling, R. F., Kitidis, V., Goldewijk, K. K., Koven, C., Landa, C. S., Landschutzer, P., Lenton, A., Lima, I. D., Marland, G., Mathis, J. T., Metzl, N., Nojiri, Y., Olsen, A., Ono, T., Peng, S., Peters, W., Pfeil, B., Poulter, B., Raupach, M. R., Regnier, P., Rodenbeck, C., Saito, S., Salisbury, J. E., Schuster, U., Schwinger, J., Seferian, R., Segschneider, J., Steinhoff, T., Stocker, B. D., Sutton, A. J., Takahashi, T., Tilbrook, B., van der Werf, G. R., Viovy, N., Wang, Y. P., Wanninkhof, R., Wiltshire, A., and Zeng, N.: Global carbon budget 2014, Earth Syst Sci Data, 7, 47-85, 2015.

Li, G., Xie, S. P., He, C., and Chen, Z. S.: Western Pacific emergent constraint lowers projected increase in Indian summer monsoon rainfall, Nat Clim Change, 7, 708-+, 2017.

Lipat, B. R., Tselioudis, G., Grise, K. M., and Polvani, L. M.: CMIP5 models' shortwave cloud radiative response and climate sensitivity linked to the climatological Hadley cell extent, Geophys Res Lett, 44, 5739-5748, 2017.

Loeb, N. G., Lyman, J. M., Johnson, G. C., Allan, R. P., Doelling, D. R., Wong, T., Soden, B. J., and Stephens, G. L. J. N. G.: Observed changes in top-of-the-atmosphere radiation and upper-ocean heating consistent within uncertainty, 5, 110, 2012.

Loeb, N. G., Wielicki, B. A., Doelling, D. R., Smith, G. L., Keyes, D. F., Kato, S., Manalo-Smith, N., and Wong, T.: Toward Optimal Closure of the Earth's Top-of-Atmosphere Radiation Budget, J Climate, 22, 748-766, 2009.

Massonnet, F., Bellprat, O., Guemas, V., and Doblas-Reyes, F. J.: Using climate models to estimate the quality of global observational data sets, Science, 354, 452-455, 2016.

Massonnet, F., Fichefet, T., Goosse, H., Bitz, C. M., Philippon-Berthier, G., Holland, M. M., and Barriat, P.-Y. J. T. C.: Constraining projections of summer Arctic sea ice, 6, 1383-1394, 2012.

Merchant, C. J., Embury, O., Roberts-Jones, J., Fiedler, E., Bulgin, C. E., Corlett, G. K., Good, S., McLaren, A., Rayner, N., Morak-Bozzo, S., and Donlon, C.: Sea surface temperature datasets for climate applications from Phase 1 of the European Space Agency Climate Change Initiative (SST CCI), Geosci Data J, 1, 179-191, 2014a.

Merchant, C. J., O. Embury, J. Roberts-Jones, E. K. Fiedler, C. E. Bulgin, G. K. Corlett, S. Good, A. McLaren, N. A. Rayner, and Donlon, C.: ESA Sea Surface Temperature Climate Change Initiative (ESA SST CCI): Analysis long term product version 1.0, NERC Earth Observation Data Centre, doi: 10.5285/878bef44-d32a-40cd-a02d-49b6286f0ea4, 2014b. 2014b.

Morice, C. P., Kennedy, J. J., Rayner, N. A., and Jones, P. D.: Quantifying uncertainties in global and regional temperature change using an ensemble of observational estimates: The HadCRUT4 data set, J Geophys Res-Atmos, 117, 2012.

NOAA: Atmospheric Carbon Dioxide Dry Air Mole Fractions from quasi-continuous measurements at Mauna Loa, Hawaii, Barrow, Alaska, American Samoa and South Pole. K. W. Thoning, D. R. Kitzis, and Crotwell, A. (Eds.), NOAA ESRL Global Monitoring Division, 2018.

O'Neill, B. C., Tebaldi, C., Vuuren, D. P. v., Eyring, V., Friedlingstein, P., Hurtt, G., Knutti, R., Kriegler, E., Lamarque, J.-F., and Lowe, J. J. G. M. D.: The scenario model intercomparison project (ScenarioMIP) for CMIP6, 9, 3461-3482, 2016.

Rayner, N. A., Parker, D. E., Horton, E. B., Folland, C. K., Alexander, L. V., Rowell, D. P., Kent, E. C., and Kaplan, A.: Global analyses of sea surface temperature, sea ice, and night marine air temperature since the late nineteenth century, J Geophys Res-Atmos, 108, 2003.

Righi, M., Andela, B., Eyring, V., Lauer, A., Predoi, V., Schlund, M., Vegas-Regidor, J., Bock, L., Brötz, B., de Mora, L., Diblen, F., Dreyer, L., Drost, N., Earnshaw, P., Hassler, B., Koldunov, N., Little, B., Loosveldt Tomas, S., and Zimmermann, K.: Earth System Model Evaluation Tool (ESMValTool) v2.0 – technical overview, Geosci. Model Dev., 13, 1179-1199, 2020.

Rossow, W. B. and Schiffer, R. A.: ISCCP Cloud Data Products, B Am Meteorol Soc, 72, 2-20, 1991.

Sanderson, B. M., Knutti, R., and Caldwell, P.: A Representative Democracy to Reduce Interdependency in a Multimodel Ensemble, J Climate, 28, 5171-5194, 2015.

Schutgens, N., Tsyro, S., Gryspeerdt, E., Goto, D., Weigum, N., Schulz, M., and Stier, P.: On the spatio-temporal representativeness of observations, Atmos Chem Phys, 17, 9761-9780, 2017.

Senftleben, D., A. Lauer, and Karpechko, A.: Constraining uncertainties in CMIP5 projections of September Arctic sea ice extent with observations, J Climate, 33, 1487-1503, 2020.

Sherwood, S. C., Bony, S., and Dufresne, J. L.: Spread in model climate sensitivity traced to atmospheric convective mixing, Nature, 505, 37-+, 2014.

Sigmond, M., Fyfe, J. C., and Swart, N. C.: Ice-free Arctic projections under the Paris Agreement, Nat Clim Change, 8, 404-+, 2018.

Susskind, J., Barnet, C., Blaisdell, J., Iredell, L., Keita, F., Kouvaris, L., Molnar, G., and Chahine, M.: Accuracy of geophysical parameters derived from Atmospheric Infrared Sounder/Advanced Microwave Sounding Unit as a function of fractional cloud cover, J Geophys Res-Atmos, 111, 2006.

Taylor, K. E., Stouffer, R. J., and Meehl, G. A.: An Overview of Cmip5 and the Experiment Design, B Am Meteorol Soc, 93, 485-498, 2012.

Tian, B. J.: Spread of model climate sensitivity linked to double-Intertropical Convergence Zone bias, Geophys Res Lett, 42, 4133-4141, 2015.

Volodin, E. M.: Relation between temperature sensitivity to doubled carbon dioxide and the distribution of clouds in current climate models, Izv Atmos Ocean Phy+, 44, 288-299, 2008.

Wang, M. and Overland, J. E. J. G. r. l.: A sea ice free summer Arctic within 30 years?, 36, 2009.

Weigel, A. P., Liniger, M., and Appenzeller, C.: Can multi-model combination really enhance the prediction skill of probabilistic ensemble forecasts?, Quarterly Journal of the Royal Meteorological Society, 134, 241-260, 2008.

Weigel, K., Eyring, V., Gier, B., Lauer, A., Righi, M., Schlund, M., Adeniyi, K., Andela, B., Arnone, E., Bock, L., Berg, P., Corti, S., Caron, L.-P., Cionni, I., Hunter, A., Lledó, L., Mohr, C. W., Pérez-Zanón, N., Predoi, V., Sandstad, M., Sillmann, J., Vegas-Regidor, J., and Hardenberg, J. v.: ESMValTool (v2.0) – Diagnostics for extreme events, regional model and impact evaluation and analysis of Earth system models in CMIP, Geosci. Model Dev. Discuss., in prep., in prep.

Wentz, F. J., Ricciardulli, L., Hilburn, K., and Mears, C.: How much more rain will global warming bring?, Science, 317, 233-235, 2007.

Wenzel, S., Cox, P. M., Eyring, V., and Friedlingstein, P.: Emergent constraints on climate-carbon cycle feedbacks in the CMIP5 Earth system models, J Geophys Res-Biogeo, 119, 794-807, 2014.

Wenzel, S., Cox, P. M., Eyring, V., and Friedlingstein, P.: Projected land photosynthesis constrained by changes in the seasonal cycle of atmospheric CO2, Nature, 538, 499-+, 2016a.

Wenzel, S., Eyring, V., Gerber, E. P., and Karpechko, A. Y.: Constraining Future Summer Austral Jet Stream Positions in the CMIP5 Ensemble by Process-Oriented Multiple Diagnostic Regression, J Climate, 29, 673-687, 2016b.

Young, A. H., Knapp, K. R., Inamdar, A., Hankins, W., and Rossow, W. B.: The International Satellite Cloud Climatology Project H-Series climate data record product, Earth Syst Sci Data, 10, 583-593, 2018.

Zhang, Y. C., Rossow, W. B., Lacis, A. A., Oinas, V., and Mishchenko, M. I.: Calculation of radiative fluxes from the surface to top of atmosphere based on ISCCP and other global data sets: Refinements of the radiative transfer model and the input data, J Geophys Res-Atmos, 109, 2004.

Table 1 Overview of recipes for emergent constraints and future projections implemented in ESMValTool (v2.0) along with the section they are described, a brief description, the required CMIP5 variables, the diagnostic scripts included and the observational datasets used in the examples. All diagnostics expect time series of monthly mean data as input. For further technical details, we refer to the GitHub repository.

Recipe name	**Section**	**Description**	**Variables**	**Diagnostic scripts**	**Observational datasets**
Section 3.1 Calculations of multi-model products~~Calculations of multi-model products~~					
recipe_multimodel_products.yml	3.1	tool to compute the ensemble mean anomaly, ensemble variance and agreement and plot the results as maps and time series	tas (example)	magic_bsc/multimodel_products.r	-
Section 3.2 Effective climate sensitivity (ECS) and transient climate response (TCR)~~Effective climate sensitivity (ECS) and transient climate response (TCR)~~					
recipe_ecs.yml	3.2	ECS using linear regression following Gregory et al. (2004)	rtmt, rtnt, tas	climate_metrics/ecs.py	-
recipe_flato13ipcc.yml	3.2	Figure 9.42 of Flato et al. (2013): (a) global mean near-surface air temperature vs. ECS; (b) TCR vs. ECS	rtmt, rtnt, tas	climate_metrics/ecs.py climate_metrics/tcr.py ipcc_ar5/ch09_fig09_42a.py ipcc_ar5/ch09_fig09_42b.py	-
recipe_tcr.yml	3.2	transient climate response (TCR) following Gregory and Forster (2008)	tas	climate_metrics/tcr.py	-
Section 3.3 Emergent constraints~~Emergent constraints~~					
recipe_ecs_scatter.yml	3.3.1.1-3.3.1.5	ECS vs. different quantities (Brient and Schneider, 2016; Lipat et al., 2017; Sherwood et al., 2014; Tian, 2015)	hur, hus, pr, rsdt, rsut, rsutcs, ta, ts, va, wap	emergent_constraints/ecs_scatter.ncl	ERA-Interim (hur, ta, va, wap), TRMM (pr), AIRS (hus), HadISST (ts), CERES-EBAF (rsdt, rsut, rsutcs)
recipe_cox18nature.yml	3.3.1.6	emergent constraint for ECS based on global temperature variability following Cox et al. (2018)	tas, tasa	climate_metrics/ecs.py climate_metrics/psi.py emergent_constraints/cox18nature.py	HadCRUT4 (tas, tasa)
recipe_ecs_multivariate_constraint_cmip5.yml	3.3.1.7	ECS vs. difference between tropical and mid-latitude cloud fraction (Volodin, 2008)	clt	emergent_constraints/ecs_scatter.py	ISCCP-D2 (clt)
recipe_wenzel14jgr.yml	3.3.2	emergent constraint on long-term sensitivity of tropical land carbon storage to climate warming (γ_{LT}) (Wenzel et al., 2014)	fgco2, nbp, tas	carbon_ec/carbon_constraint.ncl carbon_ec/carbon_gammaHist.ncl carbon_ec/carbon_tsline.ncl	NCEP (tas), GCP (nbp, fgco2)
recipe_wenzel16nat.yml	3.3.2	emergent constraint on carbon cycle - CO_2 concentration feedback (β) (Wenzel et al., 2016a)	gpp, co2	carbon_ec/carbon_beta.ncl carbon_ec/carbon_cycle_co2.ncl carbon_ec/carbon_co2-gpp-correlation.ncl	NOAA station measurements Alaska and Hawaii (co2)
recipe_seaice.yml	3.3.3	emergent constraint on YOD following Massonnet et al. (2012)	sic, areacello	seaice/seaice_ecs.ncl	HadISST (sic)
recipe_snowalbedo.yml	3.3.4	emergent constraint on snow-albedo effect following Hall and Qu (2006)	rsdscs, rsdt, rsuscs, tas	emergent_constraints/snowalbedo.ncl	ISCCP-FH (alb, rsdt), ERA-Interim (tas)

recipe_deangelis15nat.yml	3.3.5	constraint on hydrologic cycle intensification (DeAngelis et al., 2015)	hfss, lvp, prw, rlnst, rlnstcs, rsnst, rsnstcs, rsnstcsnorm, tas	deangelis15nat/deangelis1b.py deangelis15nat/deangelis2.py deangelis15nat/deangelis3.py	ERA-Interim (prw), RSS (prw), CERES-EBAF (rlnstcs, rsnst, rsnstcs, rsnstcsnorm)
recipe_li2017natcc.yml	3.3.5	emergent constraint on the future Indian summer monsoon precipitation following Li et al. (2017)	pr ,ts, ua, va	emergent_constraints/lif1.py	GPCP (pr)
Section 3.4 Climate model projections~~Climate model projections~~					
recipe_wenzel16jclim.yml	3.4.1	constraint on austral jet position in future projections	asr, ps, ta, uajet (ua), va	austral_jet/asr.ncl austral_jet/main.ncl mder/absolute_correlation.ncl mder/regression_stepwise.ncl mder/select_for_mder.ncl	ERA-Interim (ps, ta, ua, va), CERES-EBAF (asr)
recipe_toymodel.yml	3.4.2	recipe for generating synthetic observations based on the model presented in Weigel et al. (2008)	psl (example)	magic_bsc/toymodel.R	ERA-Interim (psl)
recipe_collins13ipcc.yml	3.4.3	selected figures from IPCC AR5, chap. 12 (Collins et al., 2013): mainly difference maps between future and present	areacello, clt, evspsbl, hurs, mrro, mrsos, pr, psl, rlut, rsut, rtmt, sic, snw, sos, ta, tas, thetao, ua	ipcc_ar5/ch12_calc_IAV_for_stippandhatch.ncl ipcc_ar5/ch12_calc_map_diff_mmm_stippandhatch.ncl ipcc_ar5/ch12_calc_zonal_cont_diff_mmm_stippandhatch.ncl ipcc_ar5/ch12_map_diff_each_model_fig12-9.ncl ipcc_ar5/ch12_plot_map_diff_mmm_stipp.ncl ipcc_ar5/ch12_plot_ts_line_mean_spread.ncl ipcc_ar5/ch12_plot_zonal_diff_mmm_stipp.ncl ipcc_ar5/ch12_snw_area_change_fig12-32.ncl ipcc_ar5/ch12_ts_line_mean_spread.ncl ~~emergent_constraints~~seaice/seaice_ecs.ncl~~/snowalbedo.ncl~~ seaice/seaice_yod.ncl	HadISST (sic)
recipe_seaice.yml	3.4.4	time series of sea ice area and extent, ice extent trend distributions, year of near disappearance of Arctic sea ice, emergent constraint on YOD (Massonnet et al., 2012)	areacello, sic	seaice/seaice_aux.ncl seaice/seaice_ecs.ncl seaice/seaice_trends.ncl seaice/seaice_tsline.ncl seaice/seaice_yod.ncl	HadISST (sic)

Table 2 Emergent constraints implemented in ESMValTool v2.0 and observational datasets used.

Reference	**Constrained Parameter**	**Description / observed quantity**	**Observational datasets**
Brient and Schneider (2016)	ECS	covariance of shortwave cloud reflection	HadISST (ts), ERA-Interim (hur), CERES-EBAF (rsut, rsutcs, rsdt)
Cox et al. (2018)	ECS	global temperature variability	HadCRUT4 (tasa)
DeAngelis et al. (2015)	hydrologic cycle intensification	radiative fluxes and precipitable water	CERES-EBAF (rsdscs, rsdt, rsuscs, rsutcs), RSS (prw), ERA-Interim (prw)
Hall and Qu (2006)	snow-albedo effect	springtime snow-albedo feedback values in climate change vs. springtime values in the seasonal cycle in transient climate change	ISCCP-FH (alb, rsdt), ERA-Interim (tas)
Massonnet et al. (2012)	YOD	year of disappearance (YOD) of September Arctic sea ice vs. mean sea ice extent or trend in sea ice extent	HadISST (sic)
Li et al. (2017)	future Indian summer monsoon precipitation	present-day precipitation over the tropical western Pacific	GPCP (pr)
Lipat et al. (2017)	ECS	climatological Hadley cell extent	ERA-Interim (va)
Sherwood et al. (2014)	ECS	lower tropospheric mixing index (LTMI)	ERA-Interim (hur, ta, wap)
Tian (2015)	ECS	southern ITCZ index, tropical mid-tropospheric humidity asymmetry index	TRMM (pr), AIRS (hus)
Volodin (2008)	ECS	difference between tropical and mid-latitude cloud fraction	ISCCP-D2 (clt)
Wenzel et al. (2014)	climate-carbon cycle feedback (γ_{LT})	long-term sensitivity of tropical land carbon storage to climate warming	NCEP (tas), GCP (nbp, fgco2)
Wenzel et al. (2016a)	land photosynthesis (β)	carbon cycle - CO_2 concentration feedback	NOAA station measurements Alaska and Hawaii (co2)

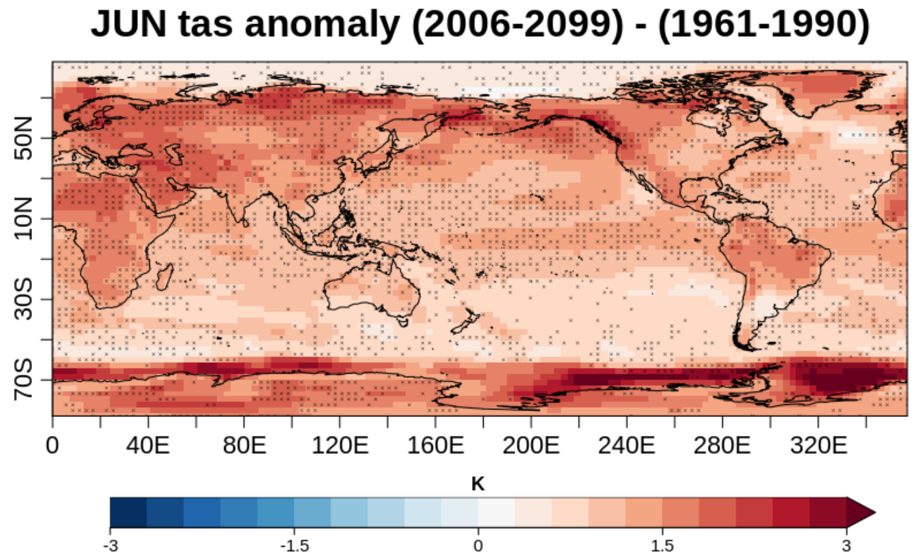

Figure 1 Multi-model mean of projected future June near-surface air temperature anomalies (2006-2099) compared with the period 1961-1990 (colors). Crosses indicate that the 80% of models agree with the sign of the multi-model mean anomaly. The models used in this example are BCC-CSM1-1, MPI-ESM-MR and MIROC5 (r1i1p1 ensembles) for the RCP2.6 scenario. All models have been regridded to the BCC-CSM1-1 grid using a linear interpolation scheme. See Section ~~3.4.2~~3.1 for details *on recipe_multimodel_products.yml*.

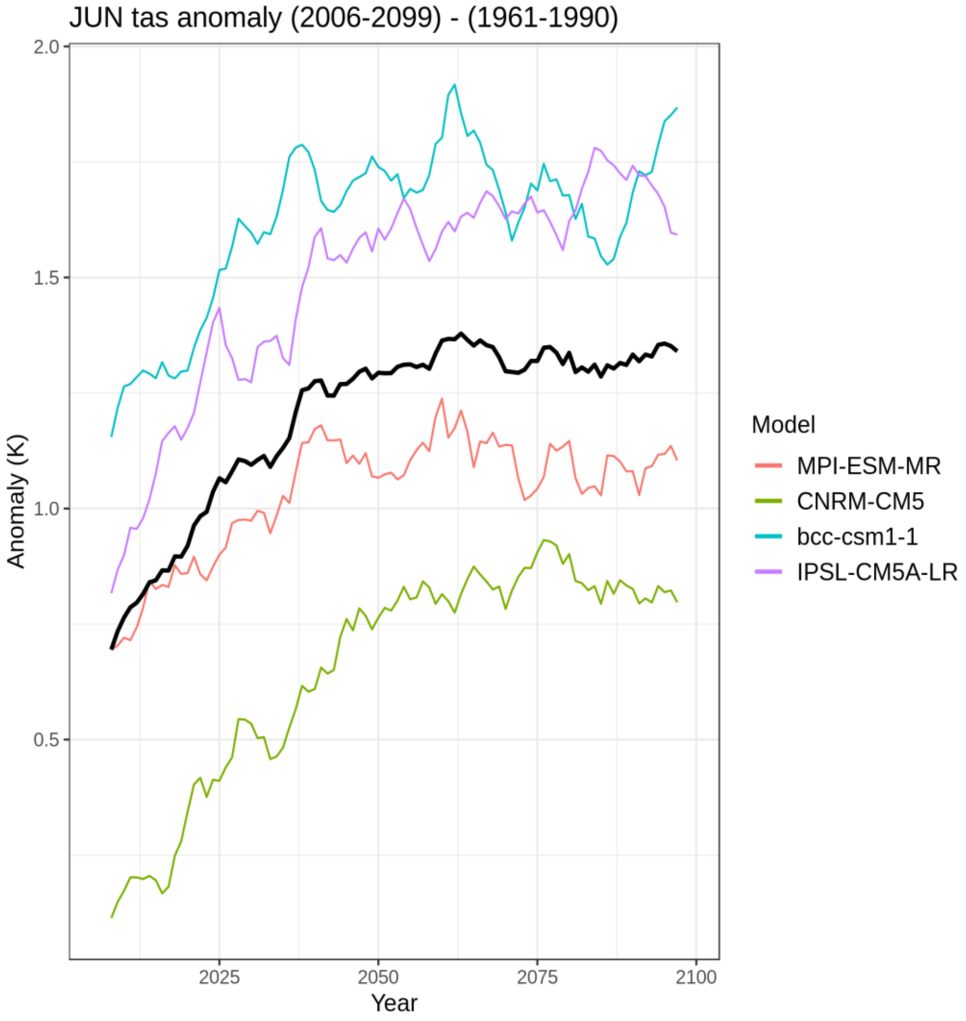

845 Figure 2 Time series of global average near-surface air temperature anomalies in June for the period 2006-2099 (RCP2.6 scenario) compared to the reference period 1961-1990. The individual models are shown as colored lines, the multi-model mean is shown in black. See Section ~~3.4.2~~3.1 for details on *recipe_multimodel_products.yml*.

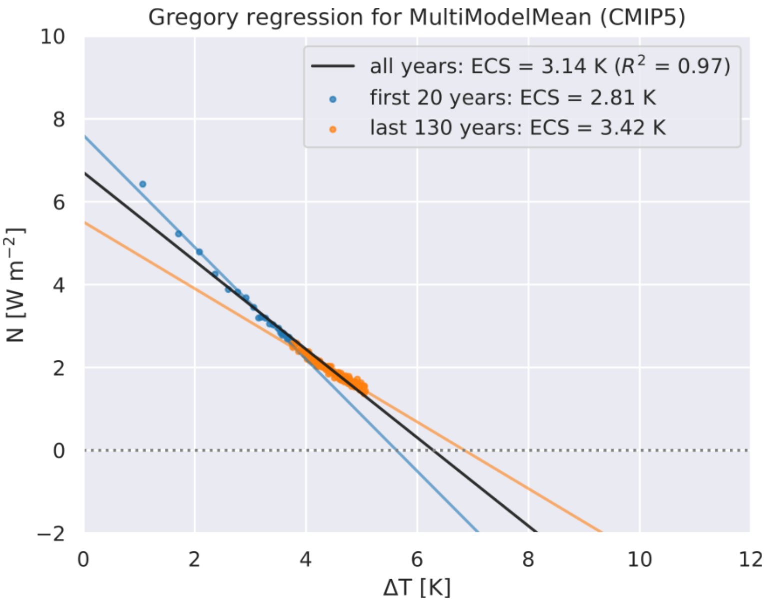

Figure 3 Gregory plot to approximate the effective climate sensitivity (ECS) (Gregory et al., 2004). Shown is the relationship between the differences in global and annual mean top of the atmosphere net downward radiative flux N (W m^{-2}) and global and annual mean near-surface air temperature anomalies ΔT (K) for the CMIP5 multi-model mean. Anomalies are calculated as difference between the abrupt4xCO2 experiment (quadrupling of CO_2) and the pre-industrial control run (piControl). The blue dots show the first 20 years of the simulation, the orange dots the last 130 years. A linear regression using only the first 20 years (blue line) instead of all 150 years (black line) results in a stronger feedback (and thus lower ECS). Using the last 130 years only (orange line) results in a weaker feedback (i.e. higher ECS). See Section 3.2 for details on *recipe_ecs.yml*.

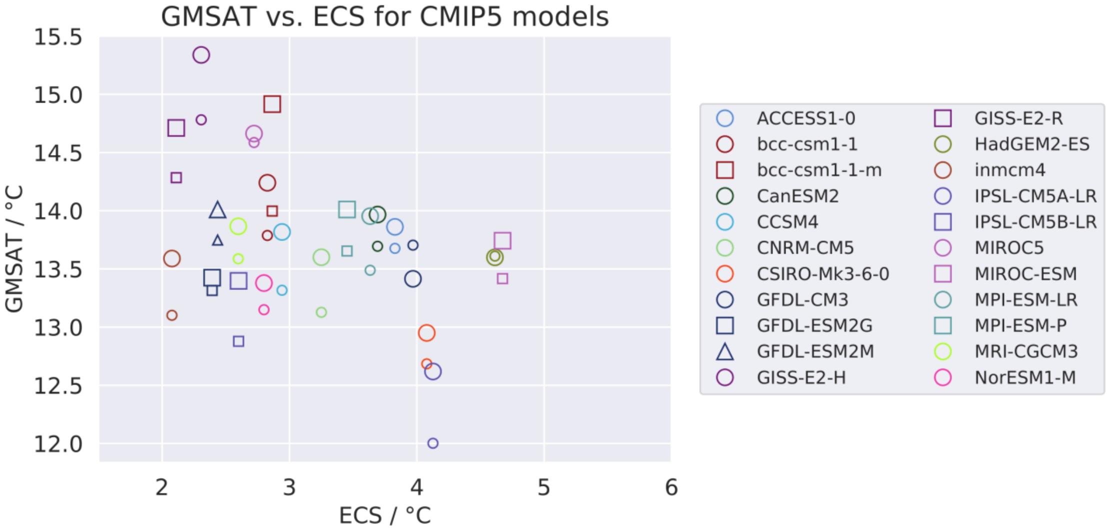

Figure 4 Globally averaged near-surface air temperature (GMSAT) of the historical period 1961-1990 vs. the effective climate sensitivity (ECS) for several CMIP5 models. Similar to figure 9.42a of Flato et al. (2013) and produced with *recipe_flato13ipcc.yml*, see details in Section 3.2.

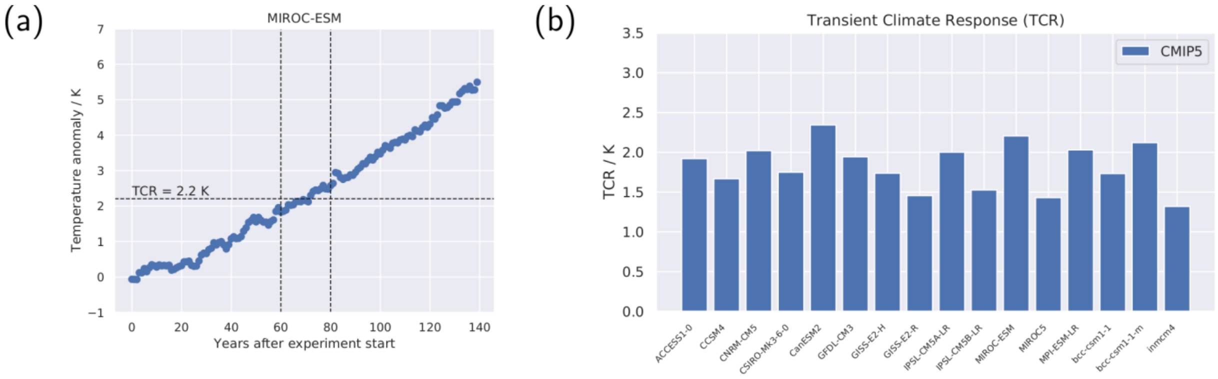

Figure 5 (a) Time series of temperature anomalies from MIROC-ESM experiment 1pctCO2 (1% increase in CO_2 per year) compared to the piControl simulation. (b) Transient climate response (in K) for CMIP5 models calculated with the method by Gregory and Forster (2008). For details on *recipe_tcr.yml* see Section 3.2.

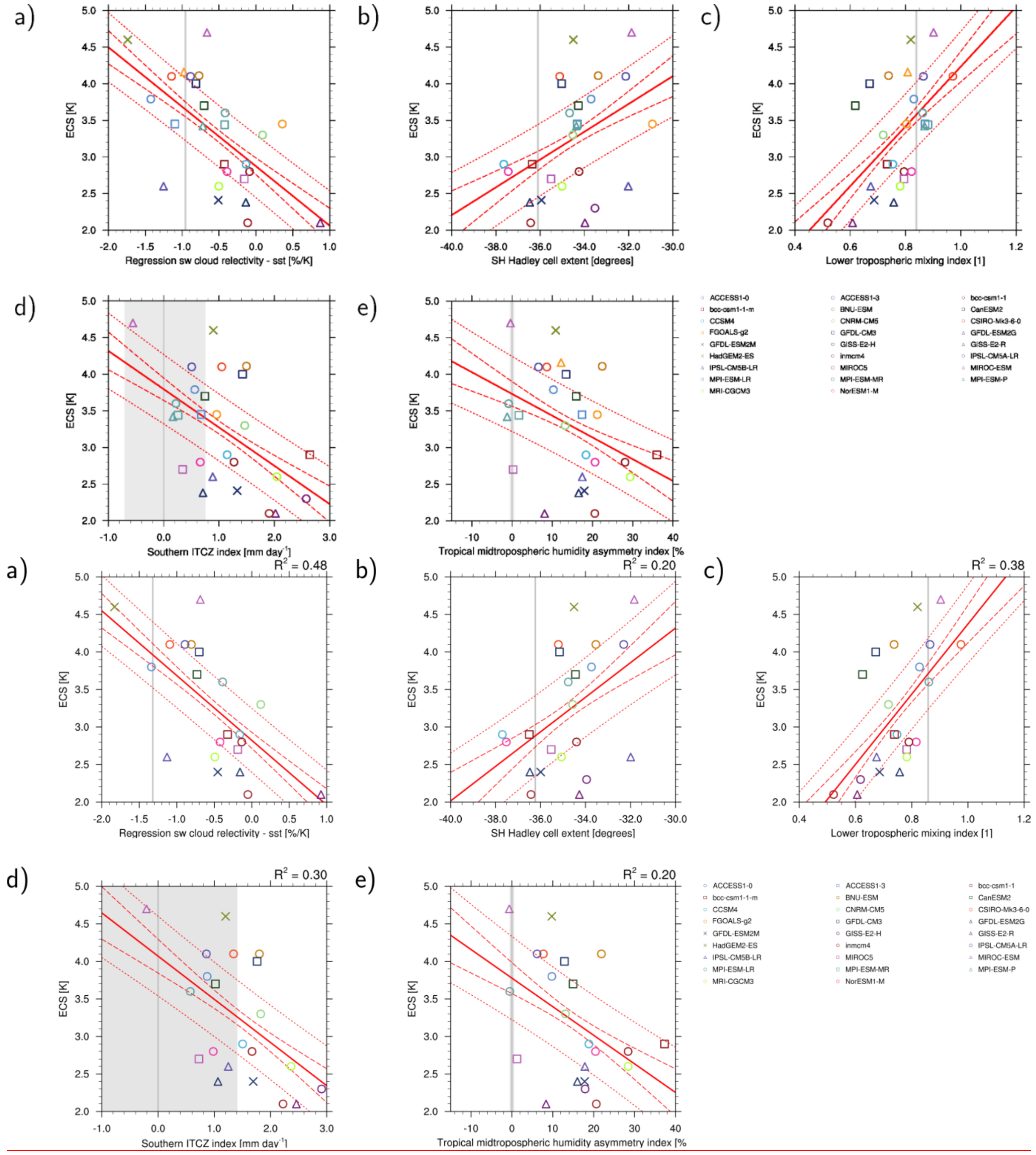

Figure 6 Scatterplots of effective climate sensitivity (ECS) vs. (a) covariance of shortwave cloud reflection (Brient and Schneider, 2016), (b) Southern Hemisphere (SH) climatological Hadley cell extent (Lipat et al., 2017), (c) lower tropospheric mixing index (LTMI) (Sherwood et al., 2014), (d) southern ITCZ index (Tian, 2015), and (e) tropical mid-tropospheric humidity asymmetry index (Tian, 2015) for CMIP5 models (symbols). The vertical gray lines represent the observations, the shaded areas in light-gray observational uncertainties (if available). The solid red lines represent the regression lines, the dashed red lines the 25% / 75% confidence intervals of the regression and the red dotted lines the 25% / 75% prediction intervals of the regression. Similar to (a) figure 6 of Brient and Schneider (2016), (b) figure 4 of Lipat et al. (2017), (c) figure 5c of Sherwood et al. (2014), (d) figure 2 of Tian (2015), and (e) figure 4c of Tian (2015). For details on *recipe_ecs_scatter.yml* see Section 3.3.1.

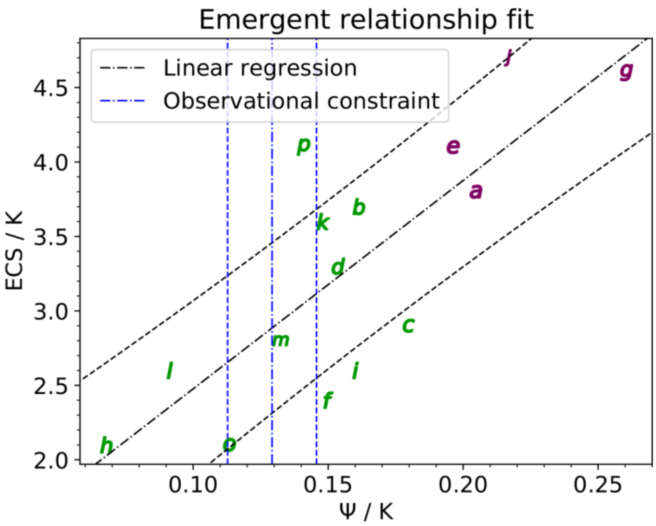

Figure 7 Emergent constraint for effective climate sensitivity (ECS). Shown is the relationship between ECS and the temperature variability metric ψ proposed by Cox et al. (2018). Letters show individual CMIP5 models (for nomenclature details see original publication) with lower sensitivity models in green and higher sensitivity models in purple. The black lines show~~s~~ the linear fit including the prediction error and the vertical blue lines indicate the observational mean and standard deviation given by the HadCRUT4 dataset. Similar to figure 2 of Cox et al. (2018) and produced *with recipe_cox18nature.yml (*see details in Section 3.3.1.6).

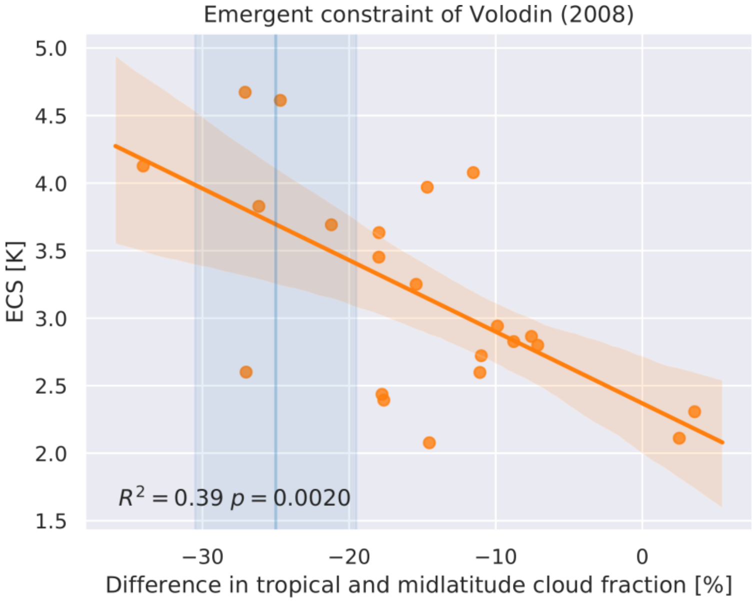

Figure 8 Effective climate sensitivity (ECS) vs. difference in total cloud cover between the tropics (28°S-28°N) and southern mid-latitudes (56°S-36°S) for CMIP5 models (orange dots). The orange line and shaded area show the linear regression line 890 and its 95% uncertainty range (estimated via bootstrapping). Together with the observational estimate (vertical blue line and shaded area), this can be used as an emergent constraint for ECS (Volodin, 2008). The observational range is based on ISCCP-D2 data (Rossow and Schiffer, 1991) and taken from Volodin (2008). Similar to figure 3a of Volodin (2008) and produced with *recipe_ecs_multivariate_constraint_cmip5.yml* (see details in Section 3.3.1.7).

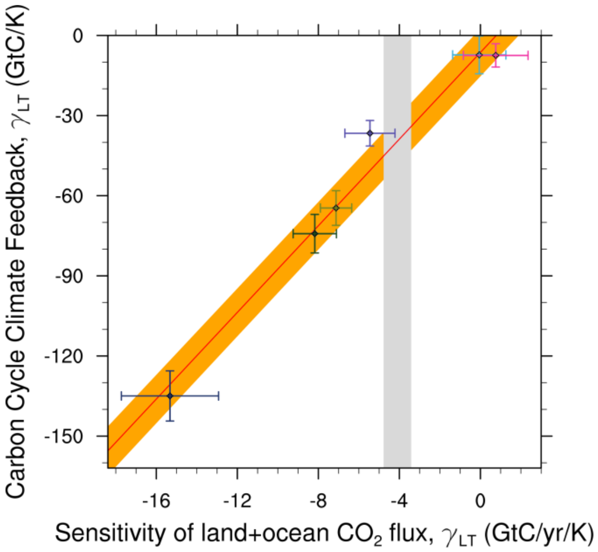

Figure 9 Relationship between long-term sensitivity of tropical land carbon storage to climate warming (γ_{LT}) and short-term sensitivity of atmospheric CO_2 to interannual temperature variability (γ_{IAV}) for CMIP5 models (markers with horizontal and vertical error bars) using the historical simulation. The red line shows the linear regression through the CMIP5 models, the vertical gray area the range of observed γ_{IAV}. Produced with *recipe_wenzel14jgr.yml*, similar to figure 5a of Wenzel et al. (2014) (for details see Section 3.3.2).

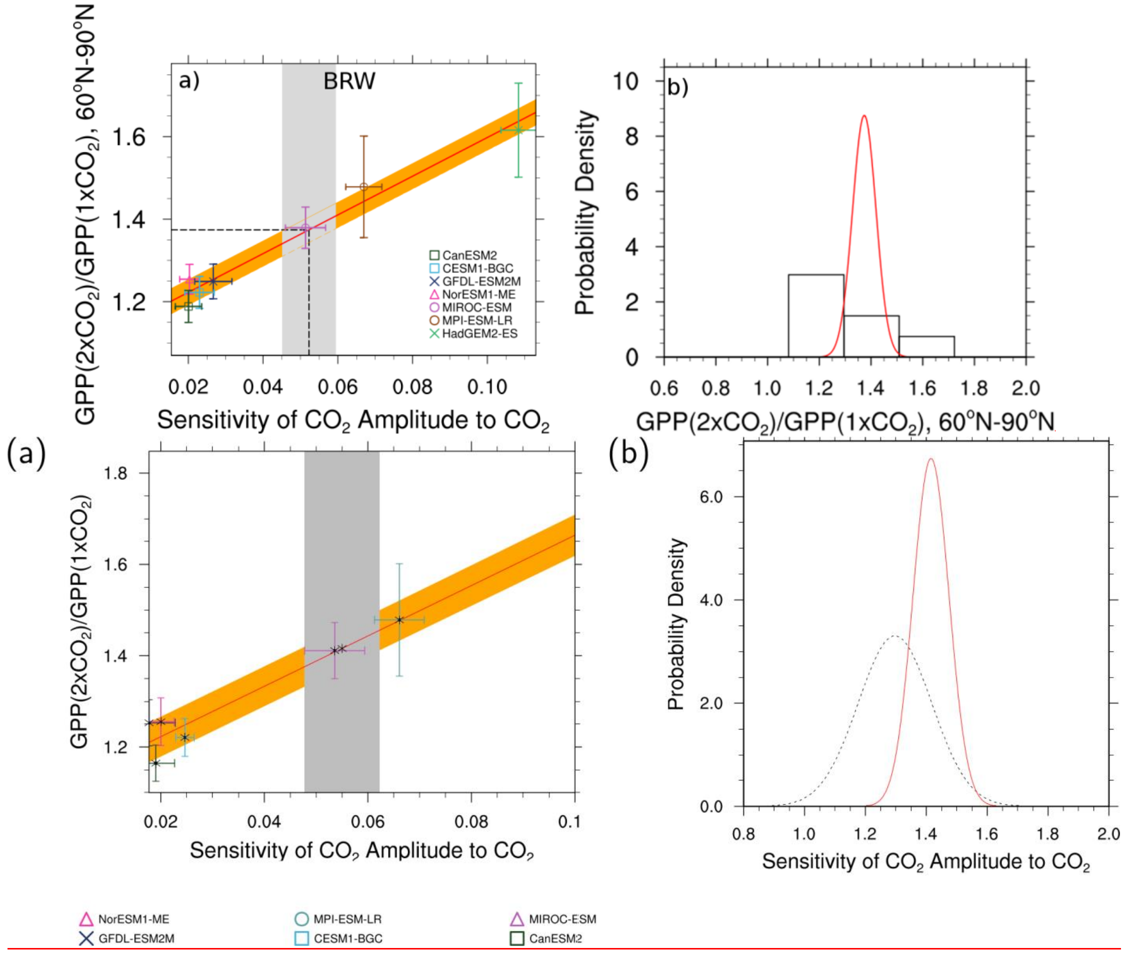

Figure 10 (a) Correlations between the sensitivity of the CO$_2$ amplitude to annual mean CO$_2$ increases at Point Barrow, Alaska (abscissa) and the high-latitude (60°N-90°N) CO$_2$ fertilization on gpp at 2 × CO$_2$. The gray shading shows the range of the observed sensitivity. The red line shows the linear best fit across the CMIP5 ensemble together with the prediction error (orange) and error bars show the standard deviation for each data point. (b) The probability density function~~histogram~~ for the unconstrained CO$_2$ fertilization of gpp (black, dotted) and the conditional probability density function arising from the emergent constraint (red). Produced with recipe_wenzel16nat.yml, similar to figure 3 of Wenzel et al. (2016a) (for details see Section 3.3.2).

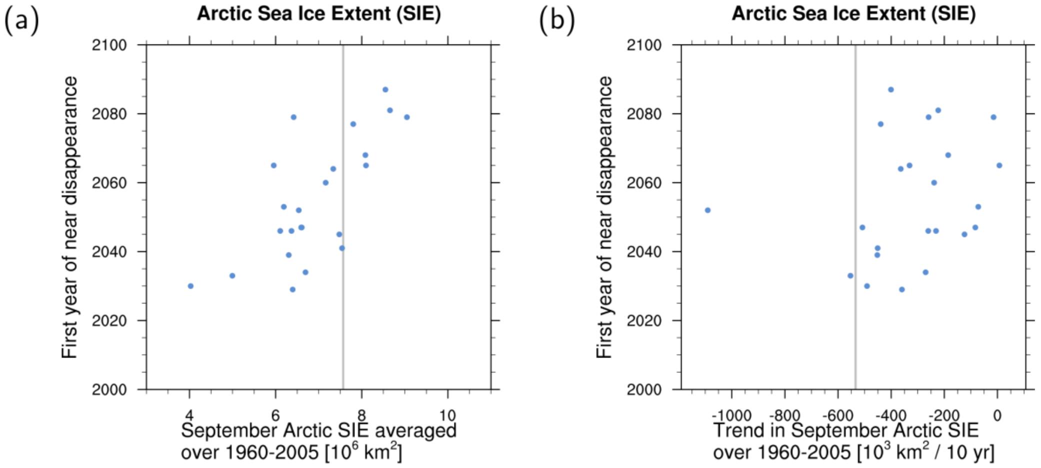

Figure 11 Scatter plot of (a) mean historical (1960-2005) September Arctic sea ice extent (SIE, million km^2) and (b) trend in September Arctic sea ice extent (1960-2005) vs. first year of disappearance for scenario RCP8.5. The vertical gray lines are calculated from observations (HadISST, Rayner et al. (2003)), similar to figures 12.31a/d of Collins et al. (2013). For details on *recipe_seaice.yml* see Section 3.3.3. 915

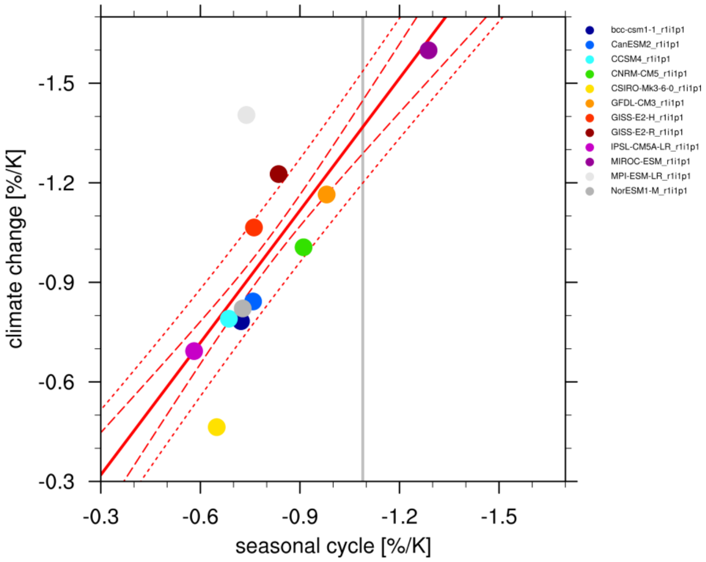

Figure 12 Scatterplot of springtime snow-albedo effect values in climate change (ordinate) vs. springtime $\Delta\alpha_s$ / ΔT_s values in the seasonal cycle (abscissa) in transient climate change experiments calculated from CMIP5 historical (1901-2000) and RCP4.5 (2101-2200) experiments. The vertical gray line shows the seasonal cycle values calculated from third generation of ISCCP radiative fluxes (ISCCP-FH, Young et al. (2018)) and near-surface air temperature from ERA-Interim (Dee et al., 2011) for the years 1984-2000. Models with higher surface albedos over NH continents poleward of 30°N typically have a larger contrast between snow-covered and snow-free areas, and hence a stronger snow-albedo feedback. Similar to figure 9.45a of Flato et al. (2013), for details on *recipe_snowalbedo.yml* see Section 3.3.4.

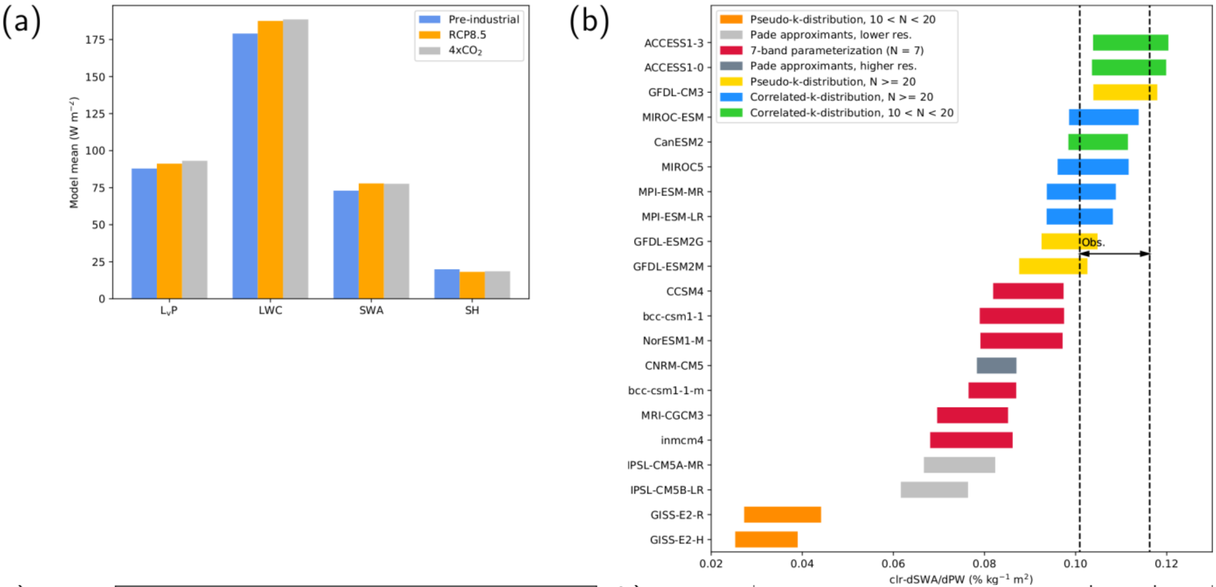

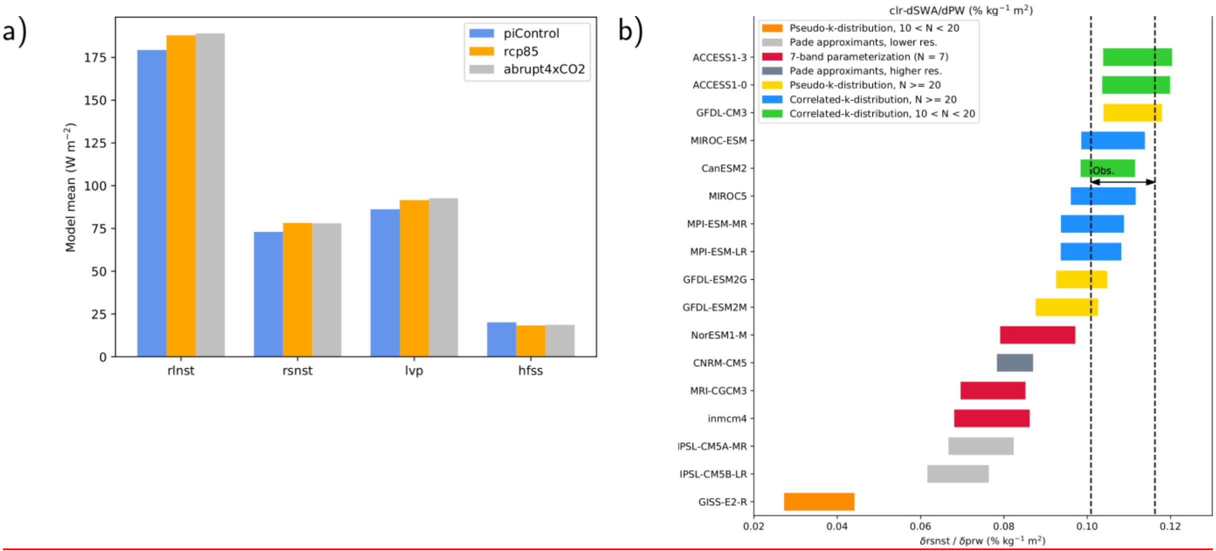

Figure 13 The atmospheric energy budget (DeAngelis et al., 2015): (a) net atmospheric longwave cooling to the surface and outer space calculated as sum of upward longwave radiative flux at TOA and net downward longwave flux at the surface (rlnst), heating from shortwave absorption (rsnst), latent heat release from precipitation (lvp) and global average multi-model mean sensible heat flux (hfss). ~~global average multi-model mean sensible heat flux (SH, CMIP5 name hfss) and derived variables LvP (latent heat release from precipitation), LWC (net atmospheric longwave cooling to the surface and outer space calculated as sum of upward longwave radiative flux at TOA and net downward longwave flux at the surface) and SWA (heating from shortwave absorption).~~ The panel shows three model experiments: the pre-industrial control simulation averaged over 150 years (blue), the RCP8.5 scenario averaged over 2091-2100 (orange) and the abrupt quadrupled CO$_2$ scenario averaged over the years 141-150 after CO$_2$ quadrupling in all models except IPSL-CM5A-MR, for which the average is calculated over the years 131-140 (gray). (b) 95% confidence interval for the slope of the regression of clear-sky ~~SWA~~rsnst normalized by the incoming shortwave flux at TOA with the water vapor path (~~PW, CMIP5 name~~ prw) over the tropical ocean (30°S-30°N), regridded to a 2.5° latitude times 2 kg m^{-2} ~~PW~~prw grid for different CMIP5 models (horizontal bars) and for data from CERES-EBAF (Kato et al. (2013); Loeb et al. (2009), ~~SWA~~rsnst) and RSS Version-7 microwave radiometer data (Wentz et al. (2007), ~~PW~~prw) together with ERA-Interim (Dee et al. (2011), ~~PW~~prw) (dotted lines). The colors indicate different parameterization schemes for solar absorption by water vapor in a cloud-free atmosphere implemented in the models. Similar to figures 1b and 4 from DeAngelis et al. (2015) and produced with *recipe_deangelis15nat.yml* (see details in Section 3.3.5).

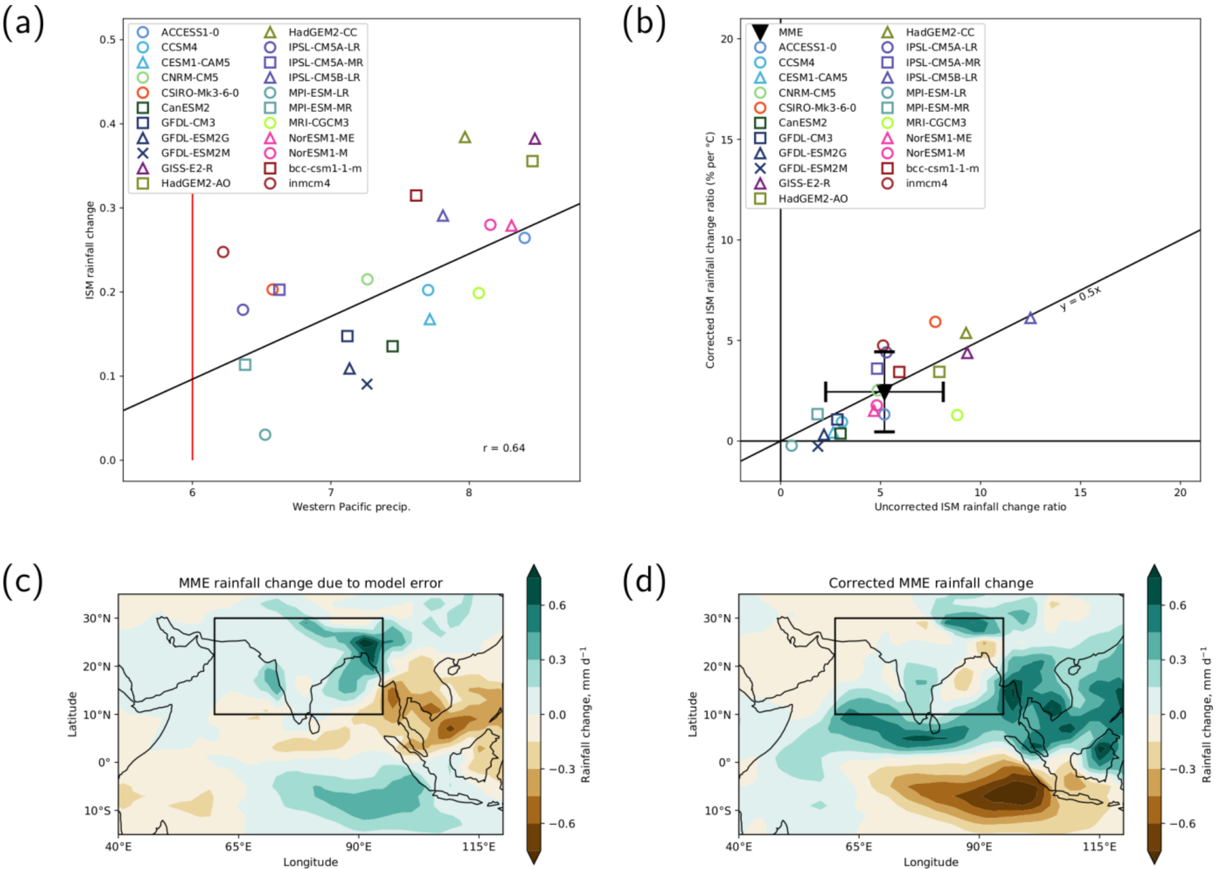

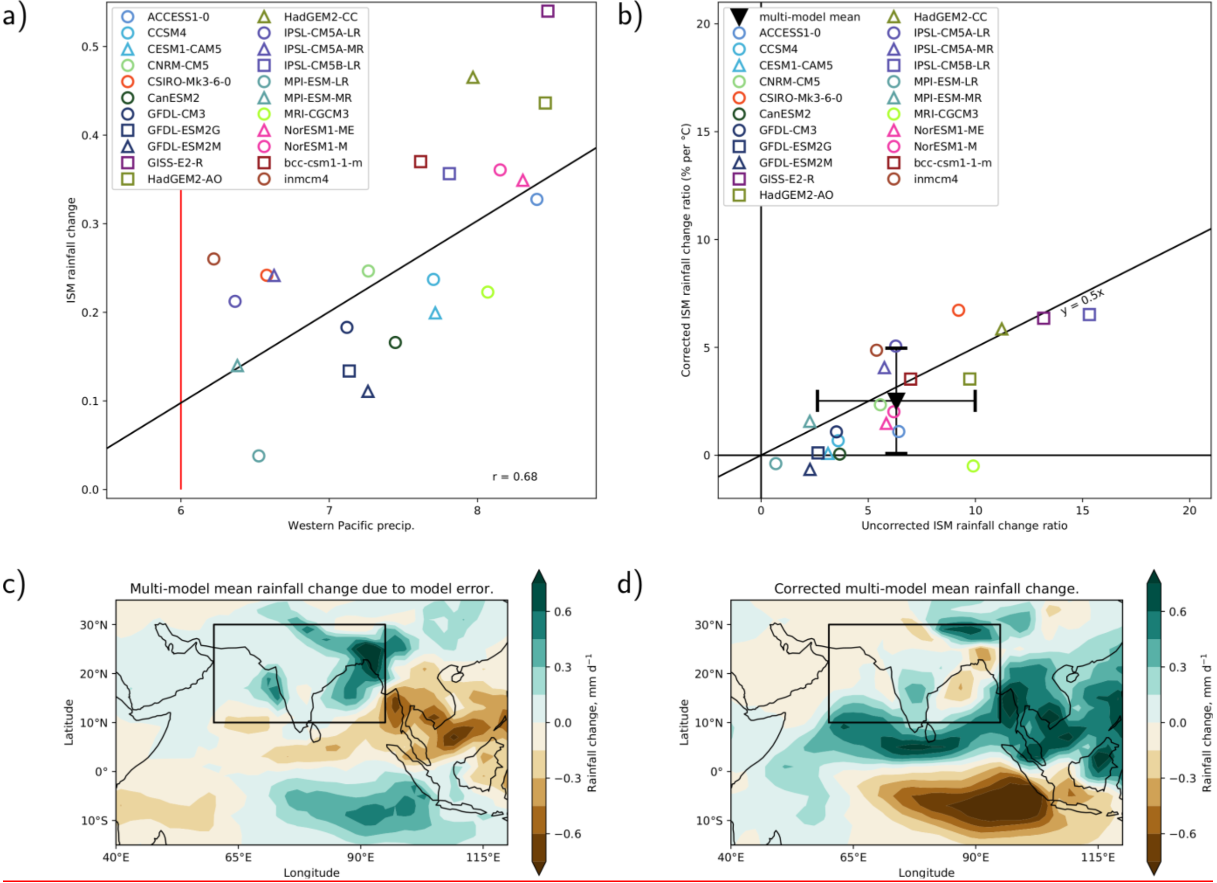

Figure 14 Correction of the Indian Summer Monsoon (ISM, 60°-95°E, 10°-30°N) rainfall projected by models for the RCP8.5 scenario based on the bias in present-day precipitation over the tropical western Pacific (140°E-170°W, 12°S-12°N). (a) Scatter plot and the linear regression (black line, with the correlation coefficient r) of the western Pacific precipitation (mm day^{-1}) from the CMIP5 historical simulations (1980-2005) and the ISM rainfall change between historical and the

RCP8.5 for the years 2070-2099 for different CMIP5 models. The red line indicates the present-day value for the western Pacific precipitation from observations as used in Li et al. (2017) estimated from the Global Precipitation Climatology Project (GPCP) dataset for 1980-1999 (Adler et al., 2003). (b) Uncorrected ISM rainfall change ratio (% per °C) vs. the corrected ratio from CMIP5 models and the multi-model mean (MME) with the standard deviations shown as error bars. The rain data are normalized by the global mean near-surface temperature change. (c) Projected multi-model mean rainfall change errors and (d) corrected multi-model mean rainfall change over the Indian Ocean. Similar to figure 2 of Li et al. (2017) and produced with *recipe_li2017natcc.yml* (see details in Section 3.3.5).

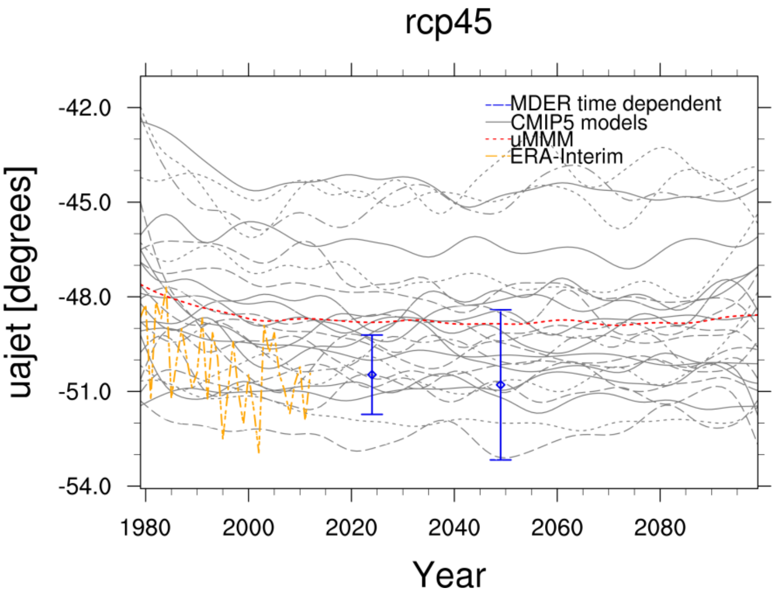

Figure 15 Time series of the austral jet position for the RCP4.5 scenario between 1980 and 2100 based on Wenzel et al. (2016b). The gray lines show individual CMIP5 models and the red dotted line the unweighted CMIP5 multi-model mean. Observationally-based estimates of the jet position from ERA-Interim (Dee et al., 2011) are represented by the yellow dashed line. Blue error bars indicate the predicted jet position by the MDER analysis (Multiple Diagnostic Ensemble Regression) for the near-term future (2015-2034) and the mid-term future (2040-2059). Similar to figure 5 of Wenzel et al. (2016b) and produced with *recipe_wenzel16jclim.yml*, see details in Section 3.4.1.

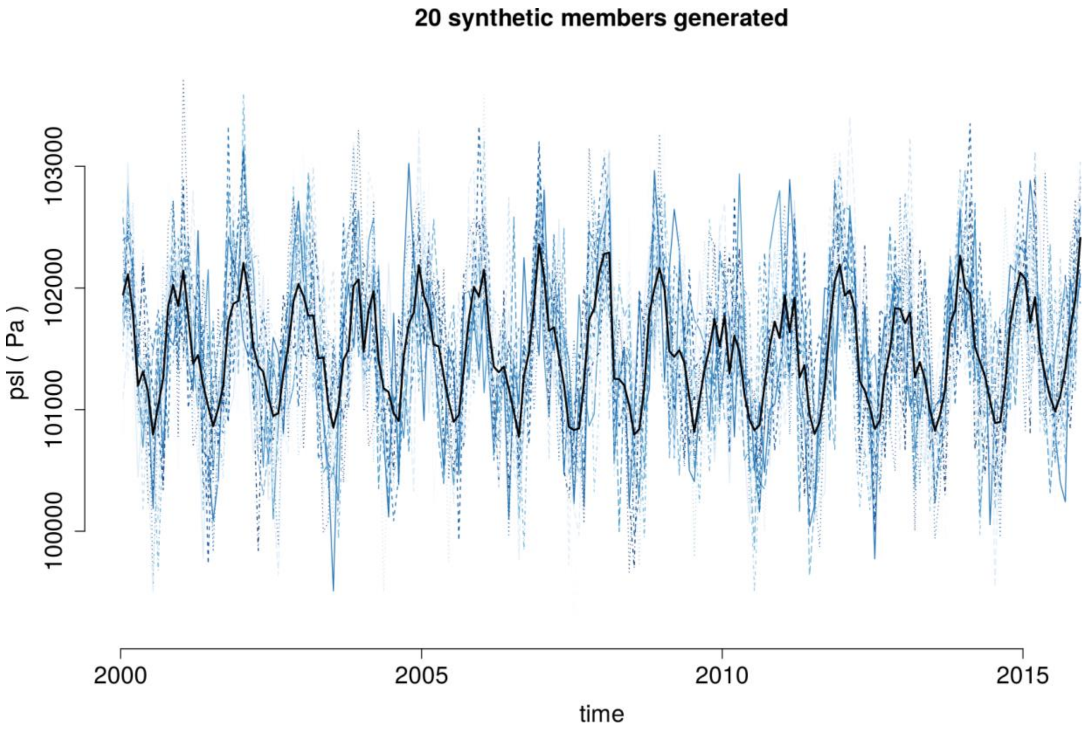

Figure 16 Example of 20 synthetic members of a single dataset ensemble generated by *recipe_toymodel.yml*. Shown are time series of surface-level pressure (psl) averaged over the region 40°E-40°W, 30°N-50°N from 2000-2015 created from monthly mean data from ERA-Interim (Dee et al., 2011). With the user providing an estimate for the standard error e.g. from differences between different observational datasets, this diagnostic can be used to investigate the effect of observational uncertainty. For details see Section 3.4.2.

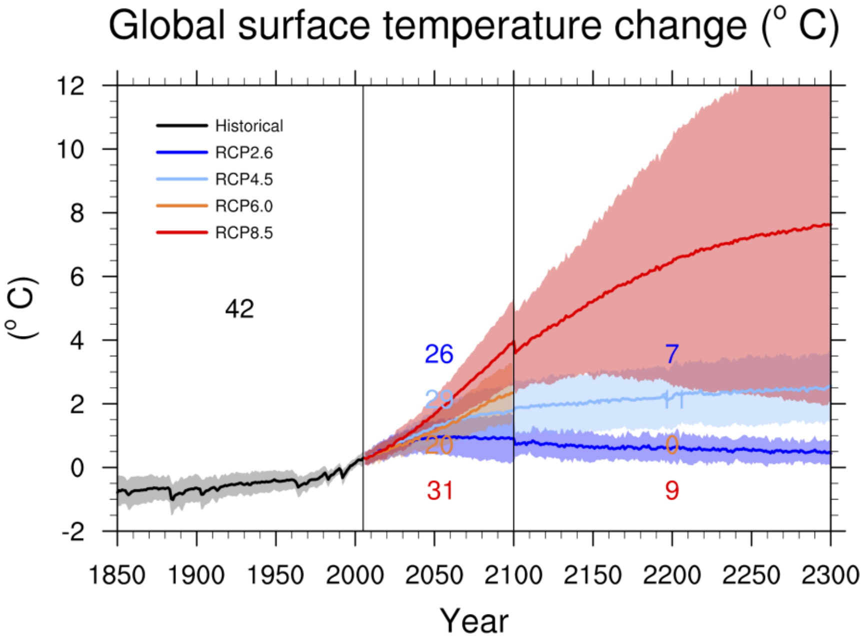

Figure 17 Time series of global annual mean surface air temperature anomalies (relative to 1986-2005) from CMIP5 models and RCP2.6, 4.5, 6.0, and 8.5 scenarios. The solid lines show the multi-model mean, the shading shows the 5 to 95% range (±1.64 standard deviations). The numbers indicate the number of models these estimates are based on. Similar to Collins et al. (2013) figure 12.5 and produced with *recipe_collins13ipcc.yml* (see Section 3.4.3 for details).

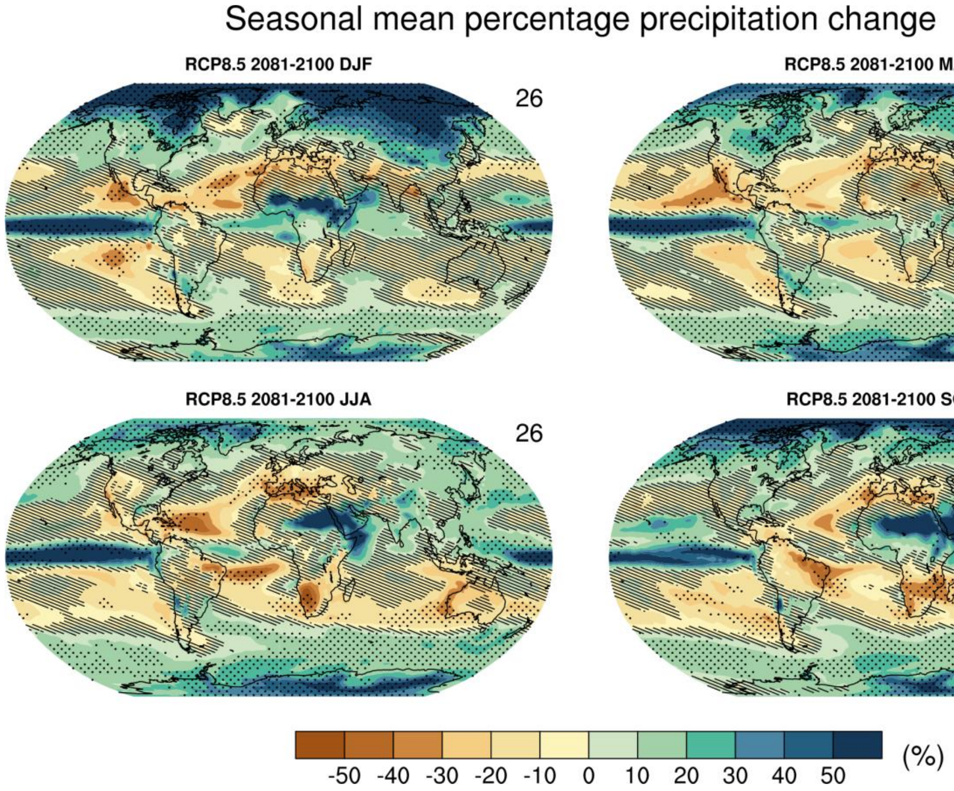

Figure 18 Global maps of seasonal mean change in precipitation from 1986-2005 (reference period) to 2081-2100 for the RCP8.5 scenario. Hatching indicates regions where the multi-model mean change is less than one standard deviation of the internal variability estimated from piControl simulations. Stippling indicates regions where the multi-model mean change is 985 greater than two standard deviations of the internal variability and where at least 90% of models agree on the sign of the change. The numbers in the upper right of each panel indicate the number of models used. Similar to Collins et al. (2013) figure 12.22 but only for one future time period. Produced with *recipe_collins13ipcc.yml* (see Section 3.4.3 for details).

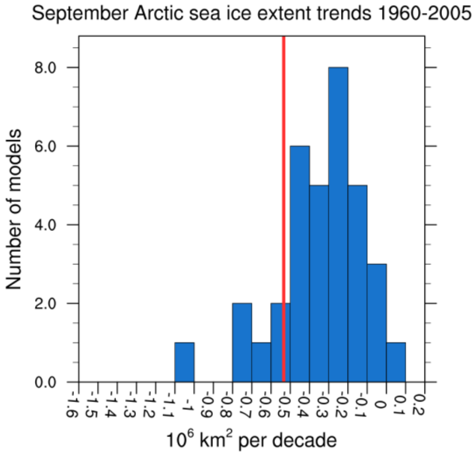

Figure 19 Distribution of trends in Arctic September sea ice extent calculated from the historical simulations (1960-2005) of 26 CMIP5 models (similar to Flato et al. (2013), figure 9.24c). An observational estimate of the trend in summer sea ice extent from HadISST (Rayner et al., 2003) over the same time period is shown by the vertical red line. Produced with *recipe_seaice.yml*, for details see Section 3.4.4.

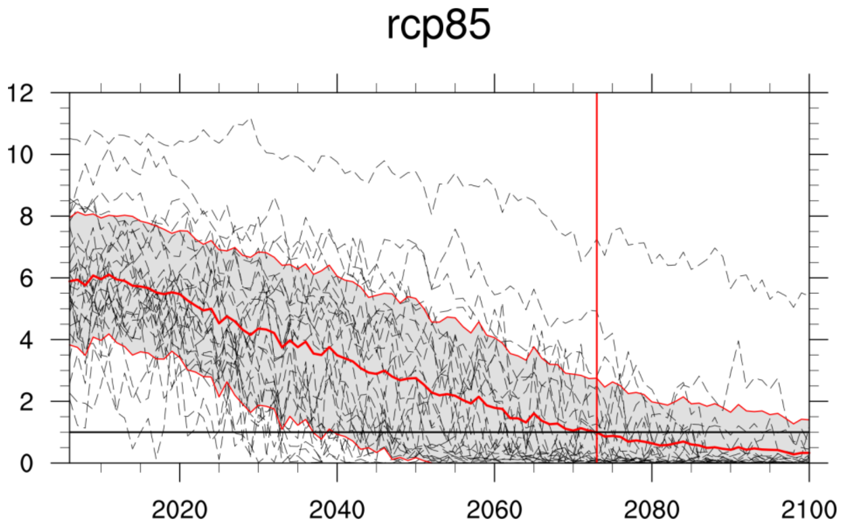

Figure 20 Time series of September Arctic sea ice extent for individual CMIP5 models (gray dashed lines), multi-model mean (thick red line) and multi-model standard deviation (area shaded between thin red lines) for scenario RCP8.5. The year of disappearance (sea ice extent below 1 million km^2) obtained from the CMIP5 multi-model mean is indicated by the 1000 vertical red line (similar to Collins et al. (2013), figure 12.31e). Produced with *recipe_seaice.yml*, for details see Section 3.4.4.